Kepler: A Search for Terrestrial Planets

K2 Handbook

KSCI-19116-002

24 July 2019

Kenneth Mighell
Jeffrey Van Cleve

Table of Contents

Kenneth Mighell (affiliate)
Digitally signed by Kenneth Mighell (affiliate)
Date: 2019.07.24 15:05:48 -07'00'

Prepared by: _____ Date _____
Kenneth J. Mighell, Science Office

JEFFREY VAN CLEVE (affiliate)
Digitally signed by JEFFREY VAN CLEVE (affiliate)
Date: 2019.07.25 09:33:59 -07'00'

Prepared by: _____ Date _____
Jeffrey E. Van Cleve, Science Office

Douglas R. Caldwell
Digitally signed by Douglas Caldwell (affiliate)
DN: c=US, o=U.S. Government, ou=NASA, ou=People, 0.9.2342.19200300.100.1.1=dacaldwe, cn=Douglas Caldwell (affiliate)
Date: 2019.07.26 10:22:55 -07'00'

Approved by: _____ Date _____
Douglas A. Caldwell, Instrument Scientist

Jeff S Coughlin
Digitally signed by Jeffrey Coughlin (affiliate)
Date: 2019.07.24 21:50:38 -07'00'

Approved by: _____ Date _____
Jeffrey L. Coughlin, Science Office Director

JESSIE DOTSON
Digitally signed by JESSIE DOTSON
Date: 2019.07.26 18:23:44 -07'00'

Approved by: _____ Date _____
Jessie Dotson, Project Scientist

1. Introduction to the *K2* Handbook

The *K2* mission began in May 2014 when the *Kepler* spacecraft was repurposed following the failure of the second of *Kepler*'s four reaction wheels in May 2013, which necessitated the end of *Kepler* mission operations. The purpose of this document, the *K2* Handbook (K2H), is to describe features of *K2* operations, performance, data analysis, and archive products that are common to most *K2* campaigns, but different in degree or kind from the corresponding features of the *Kepler* mission.

1.1 Companion Documents

The K2H is meant to be read with the companion documents listed below. Items 1–4 are retrievable from the MAST Kepler website, item 5 from the MAST *K2* website, and item 6 from the *K2* science website.

1. The *Kepler* Instrument Handbook or "KIH" (Van Cleve and Caldwell, 2016; KSCI-19033-002), which provides information about the design, performance, and operational constraints of the instrument, and an overview of the types of pixel data that are available. With the exception of failed reaction wheels and CCD modules, the flight hardware for the *K2* mission is the same as that for *Kepler*, although the performance is quite different because of the varying roll angle.
2. The *Kepler* Data Processing Handbook or "KDPH" (Jenkins et al., 2017; KSCI-19081-002). The KDPH describes how pixels downlinked from the spacecraft are converted by the *Kepler* Data Processing Pipeline (henceforth just "the pipeline") into the data products delivered to the Mikulski Archive for Space Telescopes (MAST) archive at the Space Telescope Science Institute (STScI).
3. The *Kepler* Archive Manual or "KAM" (Thompson et al., 2016; KDMC-10008-006). The KAM describes the format and content of the data products, and also how to search for them.
4. The *Kepler* Data Characteristics Handbook or "KDCH" (Van Cleve et al., 2016; KSCI-19040-005). The KDCH describes recurring non-astrophysical features of the *Kepler* data due to instrumental signatures, spacecraft events, or solar activity, and explains how these characteristics are handled by the final *Kepler* pipeline.
5. The Ecliptic Plane Input Catalog (EPIC) document or "EPIC doc" (Huber and Bryson, 2019; KSCI-19082-21). The EPIC doc describes the provenance of the positions and *Kepler* magnitudes used for target management and aperture photometry. There is also an overview of stellar properties ($M_\star$, $R_\star$, $T_\star$, etc.) for *K2* targets, with details given in Huber et al. (2016).
6. The *K2* Data Release Notes or "DRNs" describe each data processing/release, including the delivered data products, their inherent instrumental and astrophysical systematic signatures, and updates to the pipeline software since the last data processing/release. Most DRNs correspond to individual campaigns. Currently the DRNs are hosted as webpages on the *K2* Science Website by *K2* campaign number (https://keplerscience.arc.nasa.gov/k2-data-release-notes.html) and by data release number (https://keplerscience.arc.nasa.gov/k2-pipeline-release-notes.html), but ultimately will exist as one PDF per pipeline data release number with campaign-specific information, hosted at MAST (https://archive.stsci.edu/k2/data_release.html[1]).

The *Kepler* documents (items 1-4 above) were updated at the end of the *Kepler* mission and will not be revised or reissued to accommodate *K2*. The EPIC doc (item 5 above) was finalized after *K2* spacecraft end-of-flight. All *K2*-specific information will continue to be incorporated into the K2H and DRNs.

Several published papers provide more thorough treatments of *K2* flight operations (McCalmont et al., 2015), data analysis (Smith et al., 2016), and performance (Howell et al., 2014; Van Cleve et al., 2016) through roughly the first 1.5 years of science operations. The K2H will refer to these papers, but will not substantially reproduce their content. Acronyms used in this document are spelled out in Appendix B.

[1] http://dx.doi.org/10.17909/t9-t116-2c60

1.2 K2 Mission Timeline

During the *K2* mission, the *Kepler* spacecraft was constrained to point in the orbital plane, which is near the ecliptic (§2.1.2). It rotated ~81 degrees every ~83 days to observe a new field of view (FOV) for a new observing campaign (denoted C<n> for n=0 to 19). Figure 1 shows the approximate FOV boundaries for C0–C19. Typically, the telescope pointed away from the Earth (the 'anti-velocity vector' or '-VV'), but for synoptic viewing from Earth to enable simultaneous ground-based observations, some campaigns (C9, C16, C17, and C19) pointed towards the Earth (the 'positive velocity vector' or '+VV').

K2 has experienced the same kinds of science-interrupting events as *Kepler*, with comparable frequency, and thus the *K2* portion of the mission timeline (Figure 2) resembles that of *Kepler*. One qualitatively new event during *K2* operations was a spacecraft Emergency Mode in April 2016, in which the Solid State Recorder (SSR) was powered off — since this occurred between campaigns, no science data were lost.

One of the main differences between the *Kepler* and *K2* missions is that the stellar density (per square degree) was constant throughout the *Kepler* mission, but varied significantly during the *K2* mission from campaign to campaign (see Figure 3).

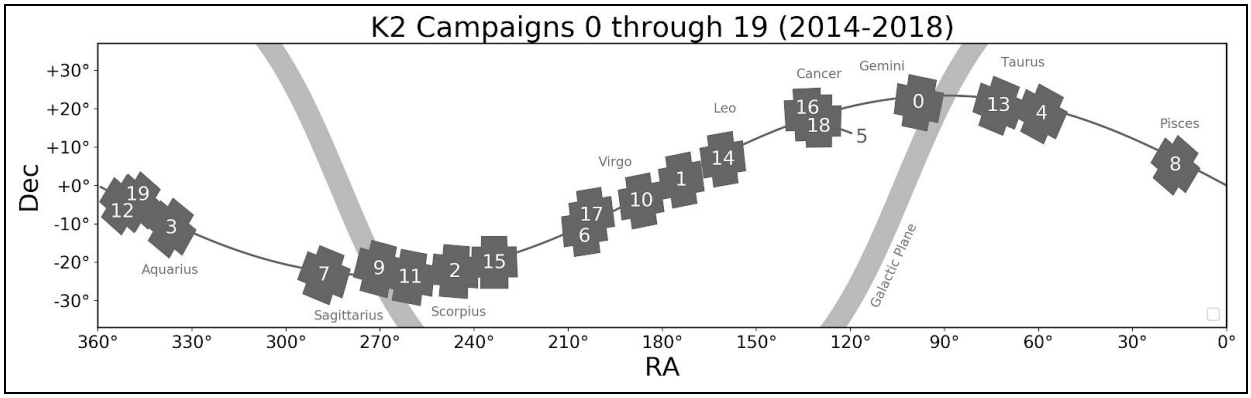

Figure 1: Approximate field of view boundaries for *K2* campaigns 0 through 19. The thin line is the ecliptic plane and the thick line is the Galactic plane.

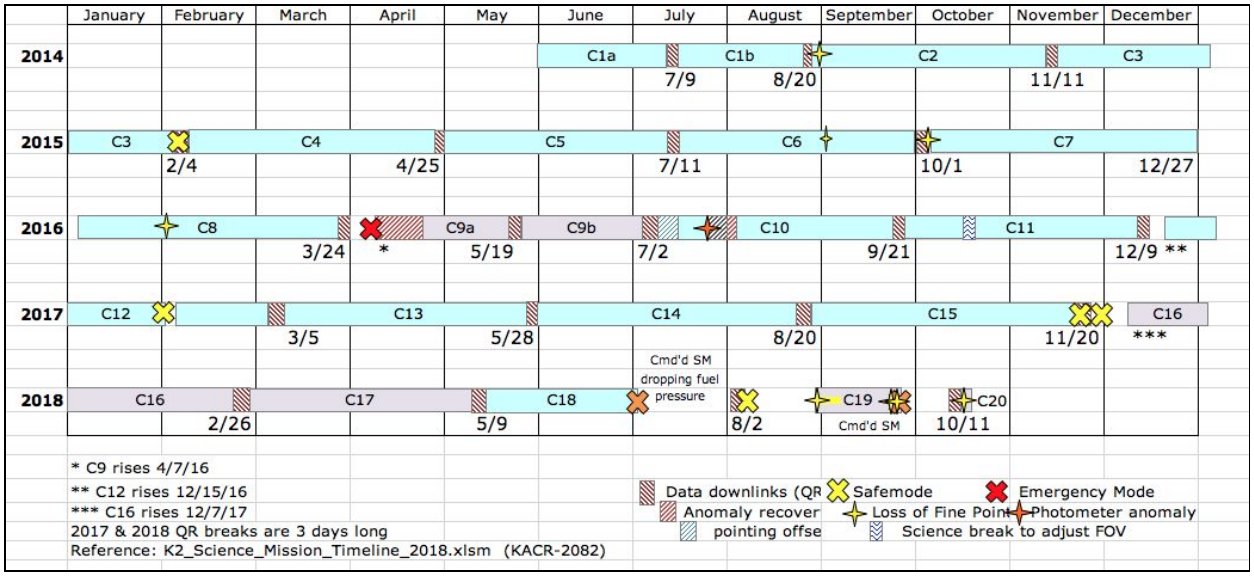

Figure 2: *K2* mission timeline showing campaign boundaries and various historical events. The +VV ('positive velocity vector') fields are shown in lavender.

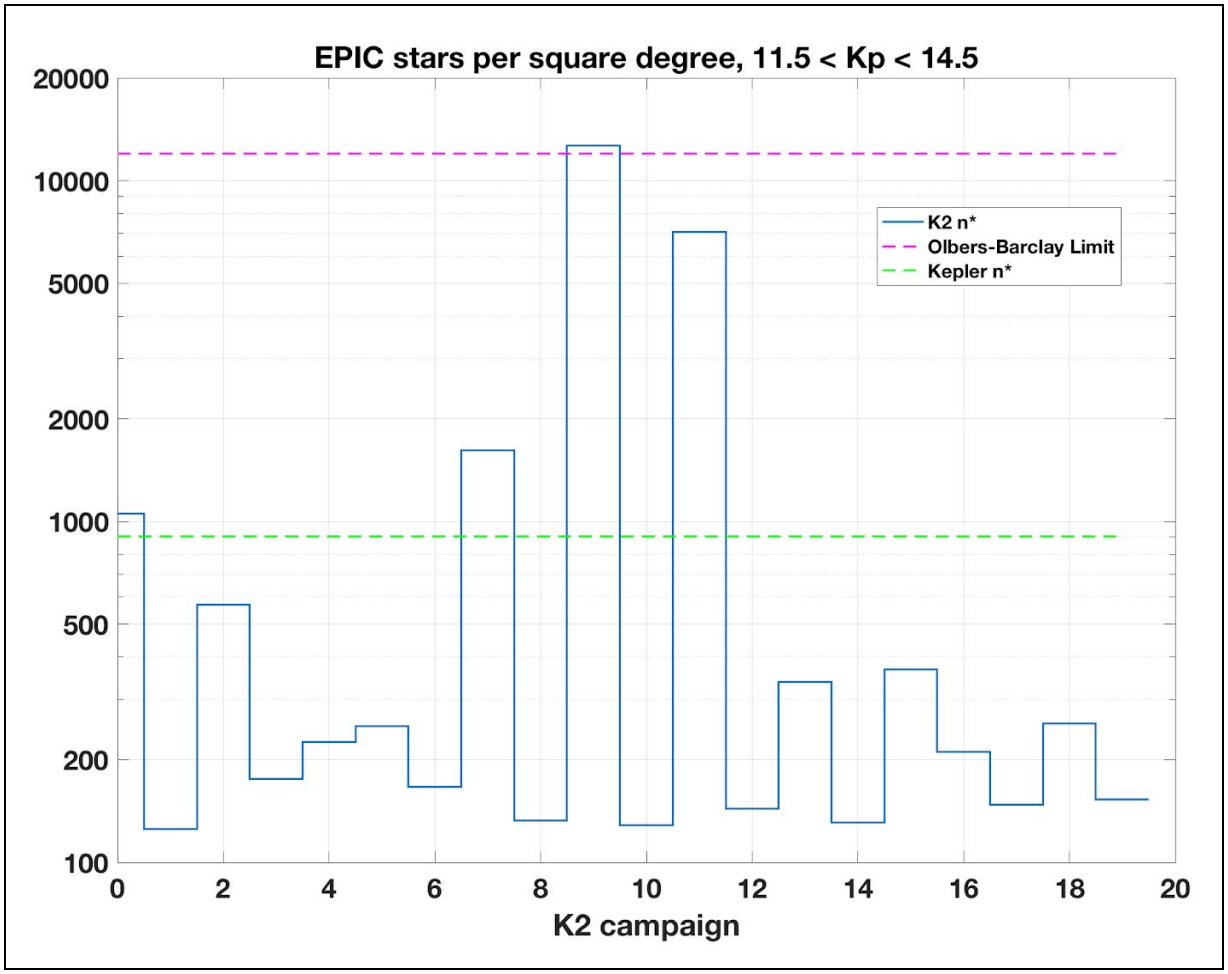

Figure 3: Observed stellar density (n*) for *K2* campaigns 0 through 19. The units are EPIC stars per square degree for 11.5 < K_p < 14.5 mag. See §3.3 for details, including the Olbers-Barclay limit.

The data for C9, C10, and C11 were processed in two parts per campaign, for various reasons. C9 was split to accommodate a larger data volume for this microlensing campaign; most of the target resources were used to tile superapertures (see §2.2.7). C10 had an initial pointing error of more than 3 pixels in boresight, as a result of a miscommunication among the flight planning team. This error was corrected after 6 days; the same set of apertures were used throughout both parts of the campaign since the apertures were designed using the correct pointing. In addition, the correctly-pointed part of C10 is itself split by an unusually long gap during which module 4 failed (see §2.1.3) and the spacecraft went into safe mode, though all the correctly-pointed data was processed together. In C11, there was a sign error in the algorithm used to correct for photon pressure emitted by the spacecraft's low-gain antenna (see §2.1.5 for details). The roll angle was corrected and updated apertures were uplinked about 3 weeks after the start of the campaign. While valid data was collected for those three weeks, without the correction and updated apertures, targets at the edge of the focal plane would have rolled out of their apertures by the end of the campaign. C1 and C2 had small pointing adjustments a few days after the start of science, but not large enough to invalidate the photometric apertures. C0 and C1 had mid-campaign breaks, but the data were processed as a single campaign. C19 had complex pointing issues due to low fuel pressure.

Campaigns in which data processing was split into two parts are designated Na/Nb in some contexts and N1/N2 in others, where N is the campaign number. For example, 10b and 102 refer to the same data set. The numerical scheme was chosen for when integer values were required; since C0 and C1 were not split, there is no practical degeneracy in this numerical scheme.

1.3 Dates and Cadence Numbers

Cadences (the frequency of observations) are defined in KDCH §1.1. The duration of long and short cadences are the same as they were in *Kepler*. Table 1 summarizes the start and end times and cadence numbers for each campaign, which may also be found in the individual DRNs.

Table 1: Dates and Cadence Numbers for all *K2* Campaigns (C0 – C19).

Campaign	Start Time of First Cadence	End Time of Last Cadence	LC Start	LC End	SC Start	SC End
0	12-Mar-2014 00:18:30	27-May-2014 16:48:13	87434	91186	2611480	2724069
1	30-May-2014 15:54:44	20-Aug-2014 20:19:37	91332	95353	2728420	2849079
2	23-Aug-2014 18:27:16	10-Nov-2014 13:27:43	95497	99352	2853370	2969049
3	15-Nov-2014 14:06:05	23-Jan-2015 18:37:04	99599	107213	2976430	3078009
4	08-Feb-2015 06:50:09	20-Apr-2015 04:32:47	103744	107213	2976430	3078009
5	27-Apr-2015 02:18:11	10-Jul-2015 22:39:43	107552	111214	3215020	3324909
6	13-Jul-2015 22:45:04	30-Sep-2015 21:11:29	111362	115224	3329320	3445209
7	04-Oct-2015 17:52:39	26-Dec-2015 08:35:28	115414	119456	3450880	3572169
8	04-Jan-2016 13:16:25	23-Mar-2016 06:48:35	119907	123759	3585670	3701259
9a/91	22-Apr-2016 14:04:59	18-May-2016 22:42:26	125243	126532	3745750	3784449
9b/92	22-May-2016 14:58:45	02-Jul-2016 22:34:52	126713	128734	3789850	3850509
10a/101	06-Jul-2016 19:45:29	13-Jul-2016 01:19:55	128925	129230	3856210	3865389
10b/102*	13-Jul-2016 01:49:21	20-Sep-2016 04:52:03	129231	132614	3865390	3966909
11a/111	24-Sep-2016 19:12:30	18-Oct-2016 02:16:19	132839	133979	3973630	4007859
11b/112	21-Oct-2016 06:17:05	07-Dec-2016 23:23:03	134134	136469	4012480	4082559
12	15-Dec-2016 20:40:49	04-Mar-2017 18:37:47	136855	140716	4094110	4209969
13	08-Mar-2017 01:35:06	27-May-2017 15:44:53	140878	144821	4214800	4333119
14	01-Jun-2017 05:06:29	19-Aug-2017 22:11:02	145045	148945	4339810	4456839
15	23-Aug-2017 22:18:11	19-Nov-2017 22:58:27	149142	153449	4462720	4591959
16	07-Dec-2017 23:01:18	25-Feb-2018 12:39:52	154331	158224	4618390	4735209
17	02-Mar-2018 00:33:12	08-May-2018 02:33:28	158445	161727	4741810	4840299
18	13-May-2018 00:44:43	02-Jul-2018 21:51:26	161969	164458	4847530	4922229
19	30-Aug-2018 15:17:06	26-Sep-2018 00:23:59	167333	168623†	5008450	5047179†

*The gap within this data (cadences 129584 and 130268) is due to the failure of module 4 (see §2.1.3).

†The last collected long cadence for C19 was 168624 (and corresponding short cadences 5047180–5047209), but were discarded in processing due to quality issues.

1.4. Full-Field Images (FFIs)

Below is a list of all the calibrated Full-Field Images (FFIs; also referred to as Full-Frame images) collected during *K2*. The file names show the integration stop time in [year][3 digit day of year][hhmmss] format, followed by the campaign number. The FFIs have the same integration parameters as an LC exposure (~29.4 min), as was the case in *Kepler*. Only one FFI was collected in campaigns 13 and 15 in order to leave enough storage space for the target cadence data. Due to indications that the spacecraft fuel tank was running very low ~50 days into C18, the collection of science data for C18 was terminated on July 2, 2018 and the spacecraft was put into a hibernation-like state until the data was downloaded at the regularly scheduled time in early August. As a result, only one FFI was collected in C18.

```
ktwo2014070234206-c00_ffi-cal.fits
ktwo2014074233223-c00_ffi-cal.fits
ktwo2014110010101-c00_ffi-cal.fits
ktwo2014157010055-c01_ffi-cal.fits
ktwo2014203150825-c01_ffi-cal.fits
ktwo2014240042843-c02_ffi-cal.fits
ktwo2014294030900-c02_ffi-cal.fits
ktwo2014331202630-c03_ffi-cal.fits
ktwo2015008010551-c03_ffi-cal.fits
ktwo2015051131033-c04_ffi-cal.fits
ktwo2015092174954-c04_ffi-cal.fits
ktwo2015127093352-c05_ffi-cal.fits
ktwo2015170131810-c05_ffi-cal.fits
ktwo2015207050529-c06_ffi-cal.fits
ktwo2015246104018-c06_ffi-cal.fits
ktwo2015290001304-c07_ffi-cal.fits
ktwo2015331045232-c07_ffi-cal.fits
ktwo2016014203204-c08_ffi-cal.fits
ktwo2016056011138-c08_ffi-cal.fits
ktwo2016119231109-c91_ffi-cal.fits
ktwo2016153221424-c92_ffi-cal.fits
ktwo2016199030108-c102_ffi-cal.fits
ktwo2016240074042-c102_ffi-cal.fits
ktwo2016279022810-c111_ffi-cal.fits
ktwo2016307123729-c112_ffi-cal.fits
ktwo2016361035629-c12_ffi-cal.fits
ktwo2017032102633-c12_ffi-cal.fits
ktwo2017079075530-c13_ffi-cal.fits
ktwo2017162122209-c14_ffi-cal.fits
ktwo2017203170143-c14_ffi-cal.fits
ktwo2017246053350-c15_ffi-cal.fits
ktwo2017344214411-c16_ffi-cal.fits
ktwo2018030100110-c16_ffi-cal.fits
ktwo2018073065336-c17_ffi-cal.fits
ktwo2018112122825-c17_ffi-cal.fits
ktwo2018143080022-c18_ffi-cal.fits
ktwo2018249002316-c19_ffi-cal.fits
ktwo2018268151041-c19_ffi-cal.fits
```

2. What's New in *K2*

2.1. Spacecraft and Instrument

2.1.1. Reaction Wheel Failures

The *Kepler* spacecraft lost the ability to precisely control its attitude while pointing at its target field in Cygnus when the second of four reaction wheels failed in May 2013 (KDCH §4.7), leading to the qualitatively different attitude control and FOV scheme for *K2*.

2.1.2. Quasi-stable Attitude Control for Ecliptic Fields of View

The engineering solution to the loss of full 3-axis control is described in the papers by the Ball Aerospace engineers who developed it (Putnam, Gravseth, & Wiemer 2016; McCalmont et al. 2015; Peterson et al. 2015) and discussed colloquially in Van Cleve et al. (2016). Briefly, since solar radiation pressure was the main perturbing torque and the spacecraft is (mostly) symmetric around the solar panel ridge, the roll axis is in unstable equilibrium when the boresight is pointed in the orbital plane (approximately the ecliptic). Residual torques then cause the spacecraft to roll, and the roll error was corrected with thruster firings every 6 hours or multiples thereof. The pointing performance is described in §3.1.

2.1.3. Module 7 and 4 failures

Module 3 failed during the *Kepler* mission, and module 7 failed between the *Kepler* and *K2* missions. Module 4 failed seven days into C10b (about 2017-07-20 07:00 UT). The cause of the module 4 failure is not known, but the sequence of telemetry faults leading up to the failure and the post-recovery behavior of the focal plane are similar to those seen around the failures of module 7 (January 2014) and module 3 (January 2010). Those failures were attributed to a blown fuse in the focal plane local detector electronics (LDE) driver boards, likely due to the failure of an upstream component creating an over-current load. The remaining 18 science modules ran well up till the end of the *K2* mission. See KIH §4 for the arrangement of modules and other detector properties.

2.1.4. Attitude Determination and Control System (ADCS) Modifications

Star trackers, Fine Guidance Sensor (FGS) CCDs in the *Kepler* focal plane, reaction wheels, thrusters, and the Attitude Determination and Control System (ADCS) software worked together to point the spacecraft. Technically they acquired the desired attitude and kept the boresight at the commanded position in the face of solar radiation torques and thermomechanical drift between the spacecraft and photometer components in the course of a campaign. McCalmont et al. (2015) gives a detailed account of how these components had to be modified in *K2* in order to restore precise control of the boresight and acceptable control of spacecraft roll. The changes that most significantly impacted *K2* operations and resulting data compared to *Kepler* were:

1. There was only one guide star per module in *K2*, instead of ten per module as was the case during the *Kepler* mission. These were carefully screened to exclude variability > 10%, close companions, extended emission, and galaxies. In some fields, suitable guide stars were so sparse that the availability of at least one guide star per module influenced the FOV setting.
2. The control bandwidth (ADCS) was increased from 0.02 Hz to 0.05 Hz prior to campaign 3, which greatly improved stability on short-cadence time scales. For *Kepler*, it was 0.1 Hz.
3. The rate at which the spacecraft rolled about the boresight was inversely proportional to the angular momentum and hence wheel speed. The wheels were at their maximum speed immediately after thrusters were fired to unload angular momentum (called "re-sats").
4. There were no longer reaction-wheel zero (speed) crossings (KDCH §5.4).

2.1.5. Coupling of Low Gain Antenna Operation to Roll Performance

Torques generated by the thermal emission of spacecraft equipment – similar to the Yarkovsky-O'Keefe-Radzievskii-Paddack (YORP) effect on asteroids (Rubincam, 2000) – were an important part of *K2*'s angular momentum budget. Switching electronics boxes on or off would shift the equilibrium orientation of the spacecraft with respect to that determined in the *K2* engineering phase, which assumed default power settings. The most salient example was the switch of Low Gain Antennas (LGAs) in C7 (see the C7 DRN). LGA1 was used for *K2* engineering operations and C0–C6, but since the antenna gain is slightly better for LGA2 in the -VV direction, LGA2 was used in C7 to compensate for the ongoing signal loss as the *Kepler* spacecraft gradually drifted away from Earth. C7 showed anomalously high roll error, which was diagnosed as a YORP effect, and the LGA1 was again used starting shortly after the beginning of C8 to restore torques to their expected values. LGA1 was used for the remainder of C8, C9, and C10. The change in roll angle needed to offset the YORP change was calculated and implemented in C11 for LGA2 operations. Unfortunately, the calculated sign of the change was wrong and C11 apertures had to be redefined in the middle of the campaign using the correct roll angle. Nominal roll torques with LGA2 operations were achieved for the latter part of C11 and C12–C15 and C18. LGA1 was used for C16, C17, and C19 since they had a +VV orientation.

2.1.6. Motion-induced Invalid Cosmic Ray Correction

The cosmic ray (CR) detection and correction algorithm (KDPH §6.3.1) was developed using the observed characteristics of *Kepler* data. The design assumes wide-sense stationary data, for which the mean is constant and autocorrelation depends only on the time separation between points. *K2* data is not wide-sense stationary, since autocorrelation is time dependent (i.e., correlation between data points separated by a fixed time interval changes with absolute time due to roll cycle). Roughly speaking, motion-induced changes in flux on a given pixel can be mistaken for signal discontinuities produced by cosmic rays. This was recognized early in the *K2* mission, and CR detection and correction were turned off for target pixels for all of *K2*. However, CR detection was enabled for the collateral data, which generated many false positive detections in the smear and virtual smear as bright star flux shifted between adjacent columns due to spacecraft motion. This generated outliers in the time series of the smear data — when the false positive detections were removed from the collateral data, then subtracting that collateral data from the science data resulted in spurious vertical bright streaks. Rather than turn off CR detection for collateral data, which would lead to a comparable amount of error from uncorrected CRs, it was found that an increase in the CR threshold substantially reduced the number of false positives in the smear and virtual smear, while continuing to do an adequate job of detecting real CRs. This higher threshold was used in C11 and subsequent campaigns, as well as reprocessed campaigns (see §2.3).

CR detection and correction was used on background pixels (pixels not in the target aperture) throughout the *K2* mission, since these apertures were designed not to contain significant stellar flux, and hence are relatively insensitive to image motion induced flux discontinuities.

2.1.7. Six-hour Thruster Firings to Restore Pointing Accuracy

During the *K2* mission, the *Kepler* spacecraft kept accurate pointing in its orbital plane (approximately the ecliptic plane) using solar photon pressure. Immediately after every 12th long-cadence exposure was complete (~6 hours), the spacecraft would autonomously decide if a very brief firing (typically 20–100 milliseconds) of the spacecraft thrusters was needed to restore pointing accuracy (see §2.1.2). The thruster firing flags (see Appendix A) denote when thrusters were fired, and are tied to the cadence data based on 16-second telemetry samples.

Since early 2018, the *Kepler* / *K2* Mission has been producing short-cadence (1-min) light curves in addition to the standard long-cadence (30-min) light curves (see §2.3). Users are cautioned that the *Kepler* pipeline detrending module (PDC), developed for use on original *Kepler* data, has not been tailored for use on short-cadence *K2* observations. Systematics due to events on fast timescales, such as thruster firings, are sometimes poorly corrected for many *K2* short-cadence targets.

2.2. Target Management

2.2.1. Overview: Monotony to Diversity

The *Kepler* mission looked at the same field in Cygnus for 4 years. The boresight was fixed, and the spacecraft rotated 90 degrees each quarter. Almost all targets and guides stars were thus simply transferred from one CCD to another for the entire mission. While targets of special interest were added, or especially uninteresting stars were removed, the target list was mostly the same throughout the mission. Targets were selected before launch from a stable *Kepler* Input Catalog (KIC), except for a small GO (Guest Observer) program. A set of optimal aperture (OA) pixels were calculated for each target, and the OA fit by the best mask selected from a finite set of masks using the TAD (Target Aperture Definition) software described by Bryson et al. (2010a, 2010b) and §3 of the KDPH. A key function called by TAD is raDec2Pix, which converts the target's astrometric RA and DEC to module, output, row, and column locations in the focal plane using the focal plane models (KAM §2.3.5) and the spacecraft boresight RA, DEC, and commanded roll angle. raDec2Pix does *not* include the roll error about the boresight that is a normal part of *K2* operations.

In contrast, the *K2* mission required a new round of target management for every campaign, including selection of a FOV, selection of targets within that FOV, and selection of aperture pixels corresponding to those targets. Targets were selected from the Ecliptic Plane Input Catalog (EPIC) which expanded to include sources in each new FOV (EPIC doc). In addition, *K2* included qualitatively new types of targets, such as Solar System Objects (SSOs), which were entirely unforeseen when *Kepler* was designed.

The strategy adopted to balance the need for code stability with the ever-changing needs of *K2* was to have a stable core of pipeline programs for target and aperture definitions (i.e., TAD; see KDPH §3) with flexible MATLAB programs to create the input for TAD, examine its outputs, trim the target list to fit the pixel budget given the estimated on-board data compression (see §3.3), and create summary reports for evaluation and approval by the Science Office and the Guest Observer Office.

While no two *K2* campaigns were exactly the same, the workflow generally followed this order:

1. The FOV was finalized after rough consideration of science targets and detailed consideration of the availability of FGS guide stars. While the RA and DEC of the FOV center was constrained to be in the ecliptic, and the roll angle was set by the stability requirement, the FOV center could be shifted in ecliptic longitude to maximize a science merit function while having at least one suitable guide star on each FOV module.
2. The EPIC was updated and science targets were selected through the GO proposal process.
3. The GO Office delivered stellar target lists, galaxy radii, bright stars with custom circular apertures, SSOs, and overrides to catalog values for proper motion and magnitude. The "stellar" targets are targets for which TAD defined the aperture, and included galaxies as well as stars.
4. Masks and apertures were designed for custom targets (see §2.2.4 – §2.2.6). The set of pixels requested for a single physical target were sometimes broken down into multiple smaller apertures, each of which had a custom EPIC ID assigned to it.
5. TAD was run to define apertures and masks for non-custom targets (stars and small galaxies). Due to a finite number of masks available, this meant that some targets — especially bright targets — had extra pixels assigned beyond what was needed to optimally capture the flux.
6. On-board data compression estimates (§3.3) yielded the number of LC and SC pixels available.
7. The LC and SC target lists with TAD-defined apertures were trimmed to meet the pixel budget, and the final TAD-defined apertures calculated. In rare instances, custom targets were removed.

2.2.2. KIC and EPIC Numbers

Kepler and *K2* use complementary target numbering schemes, collectively referred to as "*Kepler* ID," which include KIC, EPIC, and custom target numbers. KIC numbers were used only in *Kepler*, and have values < 10^8. The relatively infrequent custom targets in the *Kepler* mission have *Kepler* IDs between 10^8 and < 2.0×10^8 (KAM §2.2.1).

In *K2*, targets in the EPIC catalog have *Kepler* IDs > 2.01×10^8. Targets with *Kepler* IDs ≥ 2.00×10^8 and < 2.01×10^8 were assigned by TAD to custom *K2* targets when TAD was run, and it was anticipated that the *K2* mission would end before this finite custom target ID space was exhausted. Note that the same custom astronomical object may have multiple custom *Kepler* IDs, and may have different *Kepler* IDs for LC and SC observations if both types of data are collected. For SSOs and sky regions, these numbers are sequential for a given target and may collectively be found in MAST by searching on the custom target name. EPIC numbers > 2.01×10^8 indicate stars or galaxies that are actually in the EPIC with RA, DEC, and K_p, and which have had their apertures defined by TAD rather than the custom design process. A small fraction of EPIC objects were selected for observation by *K2*, while all EPIC objects are used by TAD to model the sky and calculate optimal apertures. Researchers can use the *K2* search tools and Custom Aperture Files (CAFs; provided for each campaign in the corresponding data release notes) at MAST to determine which *Kepler* IDs are associated with a given custom target by common name or category. Table 0 of the EPIC doc shows EPIC IDs by campaign through C20 (though only observations through C19 were taken).

The EPIC catalog has been updated to provide stellar information (temperatures, surface gravities, metallicities, radii, masses, densities, distances, and extinctions) for the targets in C1–C8 and C10–C19 (Huber et al., 2016; EPIC doc). Note that due to difficulties related to the extreme stellar density, no stellar parameters are included for C9.

2.2.3. Extra halos for Stellar Targets

In the *Kepler* mission, a "halo" of extra pixels was wrapped around the set of optimal aperture pixels in order to account for errors in catalog position, proper motion, and the small amount of image motion due to differential velocity aberration (<0.6 pixels) as attitude errors were negligible (KDPH §3). During *K2* C0, the roll errors were known to be at least a few pixels, and a conservative 10 halos were used, greatly increasing the number of pixels per target and therefore significantly decreasing the number of targets for which data could be stored. This was particularly severe for fainter stars. For example, the faintest *Kepler* star has a single-pixel optimal aperture giving a target aperture of 4x3 = 12 pixels, including one halo and one undershoot (see KIH §6.6) correction column. In C0, this target would consume 22x21 = 462 pixels, a factor of 38 increase!

As *K2* progressed, understanding and control of the flight dynamics improved, and the maximum expected roll motion decreased, so that the number of halos decreased to 6 in C1, 3–4 in C2–C4, and 2–3 in C5–C19. The halos are smaller in the center of the FOV (less than 3.4 degrees from the center) since the roll motion is proportional to the distance from the FOV center for a given spacecraft roll error — an example is shown in Figure 4 using the C18 targets. Thus, for C5–C19, the smallest *K2* aperture possible was 6x5 = 30 pixels in the inner FOV and 8x7 = 56 pixels in the outer FOV.

The *K2* apertures were sized to collect all the pixels that might be in the optimal aperture throughout the campaign; in any particular cadence, some of the target pixels may not contain useful source flux. In the pipeline, a data-driven optimal aperture is calculated and used for all cadences (the Calculate Optimal Apertures or COA program, see KDPH §7). While COA works well in a pipeline application which strives to be agnostic of scientific content, individual users may find that apertures which move or even change shape from cadence to cadence might be best for their particular science.

There were no halos on custom targets.

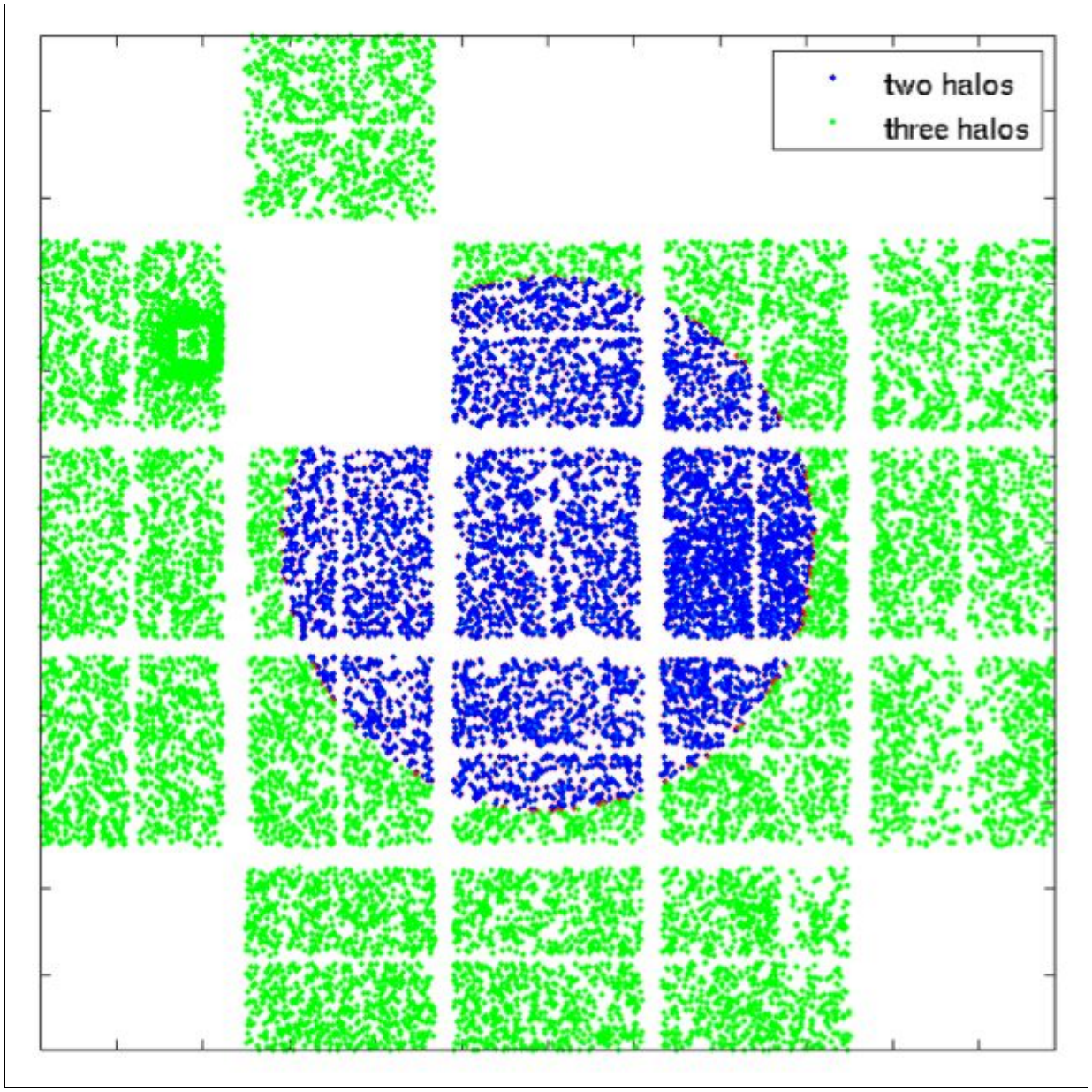

Figure 4: C18 targets plotted on the detector and colored by number of halos. Core targets (blue) had 2-pixel halos while outer targets (green) had 3-pixel halos.

2.2.4. Solar System Objects (SSOs)

Kepler was never conceived to observe Solar System Objects (SSOs), but these were common targets in *K2*. Masks are required to be defined for an entire campaign. SSOs move on the sky as seen by *K2* and their flux falls on an arc that is several pixels wide — sometimes they traverse multiple channels of the *Kepler* photometer. Defining a single mask to cover an arc was impractical, since the mask would have contained several thousand pixels per arc and been good only for that particular SSO (since each SSO's arc had a different shape). The mask pixel budget of 87,040 pixels would be quickly exhausted on SSOs alone, before attempting to fit the stellar targets! The solution was to use masks consisting of a single row (horizontal) or column (vertical) of pixels that could be tiled together to cover the arc. SSO arcs could then be composed of a mix of these horizontal and vertical masks. An example is shown in Figure 5.

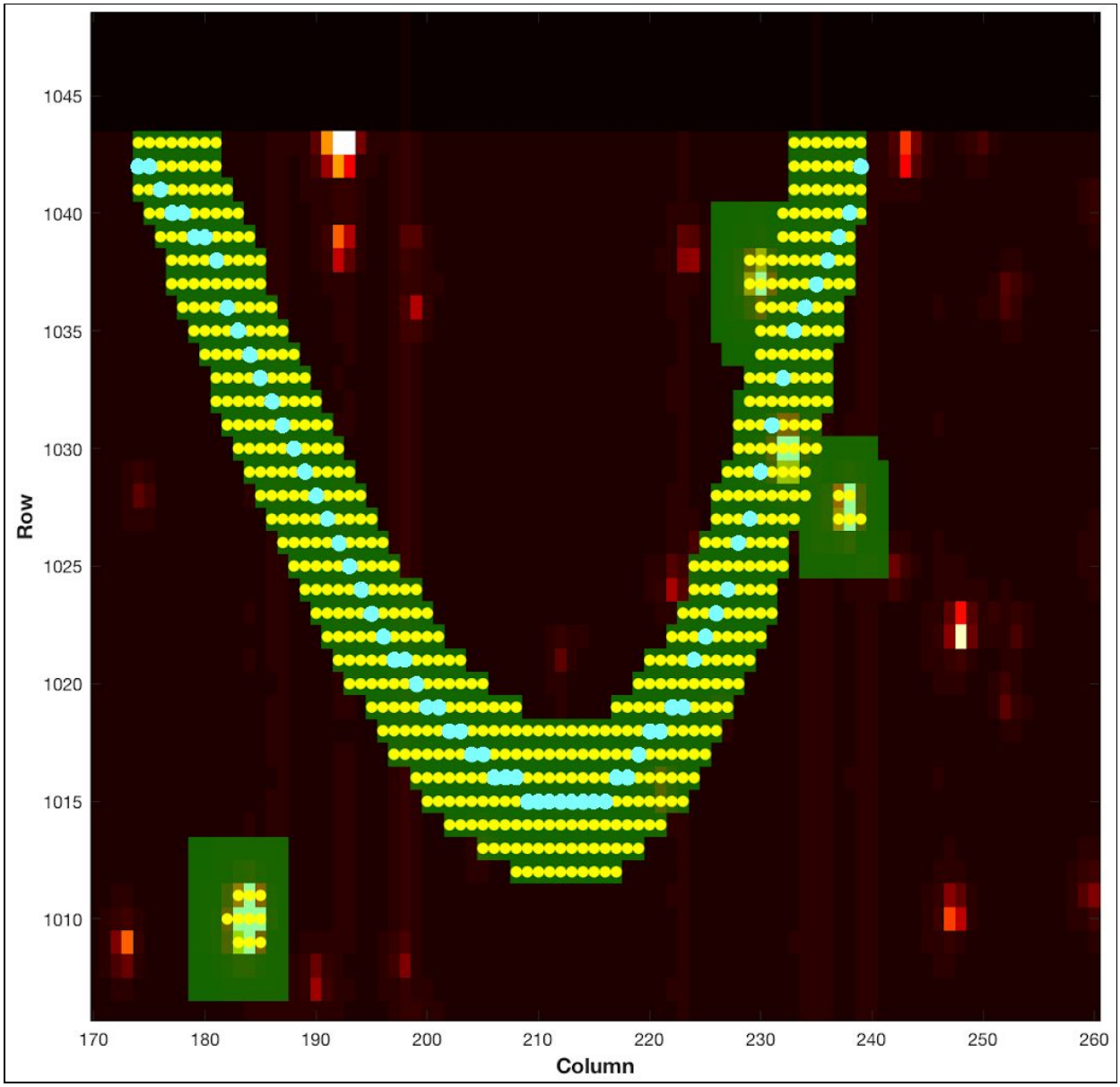

Figure 5: The set of custom apertures for the dim (K_p ~ 19.8) SSO 2000_UX34 (a Trojan Asteroid). Blue dots show the custom targets comprising the path of the SSO, yellow dots (and blue) show the optimal aperture pixels, the target pixels are colored green, and the stars are colored red/white. Roughly rectangular apertures near the arc, which do not contain a blue circle, are stellar targets.

The paths in astrometric RA and DEC of all SSOs were computed from JPL Horizons, for which the observer body ID of the *Kepler* spacecraft is -227 (in Horizons, spacecraft are assigned negative body ID numbers). K_p was then approximated from the Horizons visual magnitude or from the literature. raDec2Pix then generated the SSO path (as shown by the blue circles in Figure 5). Since the OA for stellar sources with $K_p \geq 15$ is a 2x2 box or smaller depending on the pixel response function (PRF) and subpixel registration, for faint SSOs the target pixels were "spraypainted" on the focal plane by convolving the path with a disk that had a default radius of 3.5 pixels (resulting in the yellow dots in Figure 5). This ensured the optimal pixels stayed within the aperture even as *K2* rolled. Horizontal and vertical tiles were then assigned to exactly cover the target pixels, with the unique set of masks inserted in the mask table.

For SSOs of intermediate brightness — bright enough to have optimal apertures larger than the faint stellar source limit, but not bright enough to bleed charge ($11.5 < K_p < 15$) — the target was treated as a series of instantaneous targets in a special COA run. The maximum width of the time union of optimal pixels was estimated and a convolution disk of that diameter used in the faint-source procedure. For example, this was done for Enceladus ($K_p \sim 12.3$) in C11b, with a convolution disk radius of 5 pixels.

For the brightest SSOs ($K_p < 11.5$), the special COA run results were used directly, and a set of vertical or horizontal masks defined to exactly cover the time union of OA pixels. The corresponding unique masks were inserted in the mask table. For example, this was done for Titan ($K_p \sim 8.9$) in C11b.

Use of the tiling scheme for SC SSOs could impose high data volume costs since the SC collateral (SCC) data was individually collected for each target (KIH 2.6.3.2), with no removal of duplications, and the uncompressed data volume of each SCC pixel time series was 30 times that of a LC pixel time series. For long arcs, the preferred scheme was then to cover the time union of OA pixels with a two-dimensional dedicated mask for a small number of targets (instead of one target per row/column). Duplication of SCC data was then reduced, but the mask table had to accommodate a large dedicated mask, consuming mask table pixels that could have been used to more efficiently cover the stellar targets. For example, in C8 the path of Uranus was tiled with 245 single column target definitions at long cadence but with eight 9 x 307 trapezoidal masks (and one small end cap mask) at short cadence. These masks eliminated the redundancy of SCC smear data, but there was still 8x redundancy in the SCC black data.

Data for a particular SSO may be easily located, either by family or individual names, on the MAST *K2* Data Search and Retrieval page by clicking on the “Object Type” button, and/or by searching the CAF file provided for a particular campaign in the corresponding release notes.

2.2.5. Bright Stars

TAD will compute optimal photometric apertures for bright stars ($K_p < 6$) that are exceedingly large as charge bleeds across the array, since the TAD algorithm expects that good photometry cannot be done unless all the bleeding charge is captured in the optimal aperture. Furthermore, the statistical mask design process aimed for efficient results only for stars fainter than $K_p > 9$, so the large bright star apertures were not efficiently fit, compounding the pixel consumption. A 6th magnitude star, for example, typically had an aperture containing 4000 pixels, of which ~25% are excess, i.e., not in the optimal aperture, but in the target aperture because of the limitation of the finite mask set available. To remedy this problem, many bright stars were given custom apertures that were a fixed disk of 24 to 40 pixels diameter, centered on the star. The photometry was done by modeling the wings of the PSF, with satisfactory results (Pope et al. 2016).

2.2.6. Galaxies

For extended emission from galaxies less than 40 arcsec in radius, the targets were listed in the EPIC and the stellar target list as if they were stars with an effective point source magnitude, and were given extra halos (but no undershoot columns; see KIH §6.6) to capture the additional emission. For galaxies of > 40 arcsec diameter, a custom disk of fixed radius was defined since > 10 halos (masks ~25 pixels maximum linear dimension) may have lead to inefficient mask selection in TAD.

2.2.7. Sky Regions

Science observation could be directed at an extended region of sky instead of an individual target, to look for unpredictable events such as gravitational lenses or supernovae, or to cover rich and complex areas like star clusters. If the area of the sky exceeded the typical aperture dimensions in the K_p range for which TAD generated efficient mask sets ($K_p > 9$, corresponding to masks of ~25 pixels maximum linear dimension), the region was covered with smaller masks, referred to “superapertures” or “superstamps”. Examples include the five superapertures for the gravitational lensing observations in C9, which were assembled from 1748 custom target masks, and the star cluster M67 in C5, C16, and C18.

2.2.8. Reduced Number of Nontarget Science Pixels

Because of the lower pixel budget in *K2* compared to *Kepler*, the Artifact Removal Pixels (ARPs; Van Cleve, 2008) were made spatially sparser starting in C2; C0 and C1 had a full set. There are 1174 ARP pixels per channel in *K2*, compared to 3355 in *Kepler*. The number of background pixels was also reduced after C0. No reverse-clock (RC) pixels (KIH §5.1) were collected in *K2*.

2.3. Data Processing

Users should refer to the KDPH for a comprehensive description of the *Kepler* pipeline. For *K2*, the main differences are:

- The *K2* pipeline does not perform a planet search nor planet data validation.
- Two thruster firing flags were added to the QUALITY column (see Appendix A).
- PDC uses 12 basis vectors instead of 8 to better correct the systematics due to *K2*'s roll motion.

As successive campaigns were processed, some bugs and nonoptimal parameter values were found and corrected/updated as described in each DRN. With more *K2* data in-hand, better ways to process the *K2* data were also investigated and implemented.

In early 2018, the *K2* mission began a uniform global reprocessing of the C0–C14 *K2* data with an updated, final version of the *Kepler*/*K2* pipeline; C15–C19 were processed with the same pipeline version. This effort should enhance the scientific return of the *K2* mission by providing users with a high quality, uniformly processed and documented *K2* dataset. At the time of this writing, campaigns 0, 1, 2, 3, 5, 11, 13, 15, 16, 17, 18, and 19 have been processed with this final version. The work will continue to be performed on a best-effort basis as long as mission resources are available to do so — there is no guarantee that the mission will able to reprocess every old campaign. The remaining campaigns have been prioritized by enhanced scientific return as a result of reprocessing and coupled with resource constraints, currently set as C4, C6, C7, C8, C10, C12, C14, and then C9. All data was delivered to the *K2* data archive at MAST as it was reprocessed, where the reprocessed data for a given campaign replaced the data from the older processing when searching for data via MAST's *K2* Data Search and Retrieval page and any other search interfaces. The older data remains available to users via tar archive files in the following subdirectories of the MAST browser interface: https://archive.stsci.edu/pub/k2/lightcurves/old_release_tarfiles/[2] and https://archive.stsci.edu/pub/k2/target_pixel_files/old_release_bundles/[3].

The following subsections describe the list of pipeline changes that went into effect for the global uniform reprocessing effort, and group them into two categories: Major and Minor. The Major changes affect the data at a significant level and/or are applicable to the vast majority of campaigns. The minor changes affect the data at a much less significant level and/or are applicable to only a small number of campaigns. Two figures are given below that show which campaigns are affected (or will be affected) by each change.

2.3.1. Major Changes

2.3.1.1. Improved Background Correction (Dynablack)

The *Kepler* pipeline had a feature called the Dynamic Black Correction, or "Dynablack", which is essentially a more sophisticated algorithm to perform CCD pixel-level calibration that accounts for time-varying, instrument induced artifacts in the pixel data. As shown in Figure 6 under "Improved Background Correction", Dynablack was not implemented for campaigns prior to C15, but was

[2] http://dx.doi.org/10.17909/t9-v1ae-7k16

[3] http://dx.doi.org/10.17909/t9-xp0s-kn50

implemented during the global reprocessing effort and was used to reprocess old campaigns as well as campaigns C15 through C19.

Dynablack uses the full-field images and collateral pixels to provide two main benefits compared to traditional pixel calibration:

- Correct science pixels affected by thermally dependent crosstalk from the fine guidance sensors.
- Identify rolling-band artifacts (see §6.7 of the KIH) with flags in the target pixel files.

Users can track rolling-band artifacts using the new RB_LEVEL flags in the FITS files. See §A.1.1 of the *Kepler* Data Release 25 Notes and §2.3.2 of the KAM for information on how to interpret and utilize the RB_LEVEL flags. In-particular, users should note that the RB_LEVEL test at the two shortest durations, 3 cadences (1.5 hours) and 6 cadences (3 hours), are overly sensitive to instrument noise and do not offer a reliable indicator of the presence of rolling band pattern noise. The binary "Rolling Band Detected" QUALITY and SAP_QUALITY flags (bits 18 and 19; see Appendix A) in target pixel files and light curve files are based on a rolling band detection at *any* of the test durations indicated by the FITS header keywords RBTDURi (where i ranges from 1 to 5); *these two flags do not provide a reliable indicator of the presence of rolling band pattern noise*. Note that the correct units for RBTDURi is the number of long cadences, and is mislabeled in both the *Kepler* DR25 and the latest *K2* C2, C13, C15, and C16 FITS files. In summary, the RB_LEVEL flags at durations greater than 6 cadences (3 hours) provide the best indication of the presence of rolling band artifacts.

	C0	C1	C2	C3	C4	C5	C6	C7	C8	C9	C10	C11	C12	C13	C14	C15	C16	C17	C18	C19
Improved Background Correction	✓	✓	✓	✓		✓						✓		✓		✓	✓	✓	✓	✓
Better Identification of Bad Spacecraft Pointing	✓	✓	✓	✓		✓						✓		✓	✓	✓	✓	✓	✓	✓
Better Identification of Good Spacecraft Pointing	✓	✓	✓	✓		✓						✓		✓		✓	✓	✓	✓	✓
Improved Cosmic Ray Correction	✓	✓	✓	✓		✓						✓	✓	✓	✓	✓	✓	✓	✓	✓
Short Cadence Lightcurves Produced	✓	✓	✓	✓		✓						✓		✓		✓	✓	✓	✓	✓

Figure 6: The status of major processing features for each campaign as of June 3, 2019. Check marks indicate that the feature is present in the currently available data for that campaign. Blue check marks are features/improvements added as a result of the global uniform reprocessing effort. The *K2* mission will endeavor, on a best-effort basis, to fill in as many of the blank boxes as possible as the global uniform reprocessing effort continues.

2.3.1.2. Not in Fine Point Flag

Throughout *K2*, software on-board the spacecraft would record when it considered itself not in fine point. The pipeline would flag these cadences as "Spacecraft is not in fine point" (QUALITY flag bit #16, decimal=32768) and the data would be gapped in both SAP flux and PDCSAP flux lightcurves. Starting with C14, a change in the on-board software resulted in additional cadences being flagged as "Spacecraft is not in fine point". Before this change, but especially after this change, it was noticed that the "Spacecraft is not in fine point" flag was set on cadences that actually contained good data where the spacecraft pointing was acceptable for science observations.

The "Spacecraft is not in fine point" flag was used for all campaigns prior to C15. For C15–C18 and all reprocessed campaigns, it is ignored in the pipeline. (It was used for C19 due to erratic pointing as a result of fuel exhaustion.) See the next section, "Coarse Pointing Flag", for how cadences with poor pointing are now appropriately handled in the pipeline.

2.3.1.3. Coarse Pointing Flag

As shown in Figure 6, under “Better Identification of Bad Spacecraft Pointing”, for campaigns C14–C19, and all reprocessed campaigns, the pipeline is now using the "Spacecraft is in coarse point" flag (QUALITY flag bit #3, decimal=4; see Appendix A) to identify cadences with significant pointing error. This flag is set by mission personnel based on the measured pointing error using high-frequency sub-cadence telemetry. If 4 or more continuous short cadences each exceed 1.5 pixel pointing error during exposure, they are flagged. Similarly, if 4 or more continuous long cadences each exceed 1.5 pixel pointing error during exposure, they are flagged. Additionally, if any short- or long-cadence exceeds 2.5 pixel pointing error during exposure, it is flagged. The pipeline treats these "coarse-point" cadences by gapping them in the PDC lightcurves for the flagged cadences. The mission found that implementing this flag significantly improved the measured precision of the PDC lightcurves, both as a result of eliminating flux outliers due to poor pointing and PDC being able to focus more of its detrending power on correcting broad systematics and not single outliers. Especially for C14–C19, the mission recommends that users look to QUALITY flag bit #3 as an indicator of poor spacecraft pointing.

2.3.1.4. Cosmic-Ray Threshold

As discussed in §2.1.6, the *Kepler* pipeline employs an algorithm to detect when cosmic rays impact the collateral area of the CCD. The collateral area is used to calibrate the pixel-level data, so the algorithm corrects the collateral area to account for cosmic rays when they are detected to ensure that the pixel-level data are properly calibrated. The original *Kepler* pipeline was not designed to work with significant (> 1 pixel) motion, especially in the presence of very bright objects, which were both common to *K2* (see §2.1.6). As a result, the algorithm sometimes falsely triggers, which results in an artificial suppression of the collateral smear data, and thus an under-correction of all pixels in an affected column. The net effect is the presence of bright columns in affected cadences. This effect was not noticed to be significant until many campaigns had been processed, and varies significantly per campaign and channel.

After investigation, the mission determined the most effective course of action was to raise the threshold of the collateral cosmic ray detector from 4σ to 7σ (standard deviations), which struck a balance between minimizing false detections while still detecting and correcting for significant, real cosmic ray events. This change improves photometric precision by reducing the number of flux outliers in the lightcurves. As shown in Figure 6 under “Improved Cosmic Ray Correction”, the cosmic ray threshold was set to 4σ for C0–C10 and 7σ for C11–C19 and all reprocessed campaigns.

2.3.1.5. Short Cadence

The *Kepler* pipeline corrects short-cadence PA light curves by interpolating from the long-cadence cotrending basis vectors (CBVs) that are produced as a result of long-cadence PDC. This method was not designed with the significant motion and resulting systematics that arise in *K2* data, and as a result often does a poor job of detrending *K2* short-cadence data. For this reason, beyond an initial inspection based on C2, the mission initially did not attempt to produce short-cadence *K2* light curves as part of its processing for C0–C14, as shown in Figure 6. Note that even when the *K2* mission did not initially deliver short-cadence lightcurve files, short-cadence target-pixel files were delivered (along with the long-cadence lightcurve files and the long-cadence target-pixel files).

As part of the global reprocessing effort, the *K2* mission revisited the prospect of producing short-cadence light curves by doing so for C15. In consultation with *K2* users, the mission decided that despite the often poor detrending, there was value in having short-cadence light curves available for at least an initial inspection, especially given that currently short-cadence light curves are not produced for most short

cadence targets as part of the community-delivered high-level science products. The hope was that these pipeline short-cadence light curves may be used for initial inspection of the short-cadence data, which might prompt users to perform their own short-cadence detrending, or better adapt the existing long-cadence Cotrending Basis Vector (CBV) files for use in detrending the short-cadence data.

For C15–C19, as well as for all reprocessed campaigns, short-cadence light curves have been delivered. (Note that no lightcurves, including short-cadence, will be delivered for C9). Users are strongly cautioned that no work was done to adapt the *Kepler* pipeline's detrending module (PDC), developed for *Kepler* data, to work well on short-cadence *K2* data. *Thruster firings are especially poorly corrected for most short-cadence targets, and other systematic features may not be corrected well.* See Figure 11 for an example of remaining systematics in short-cadence data around thruster firings. Note that some targets *do* have adequate detrending in short-cadence, and even in cases of poor detrending, short-term astrophysical variation can be seen for targets where such astrophysical variation exists. For example, Figure 7 shows the C15 long- and short-cadence PA and PDC lightcurves for the AM CVn type binary HP Lip, where its ~18 minute periodic variations are readily apparent in the short-cadence data.

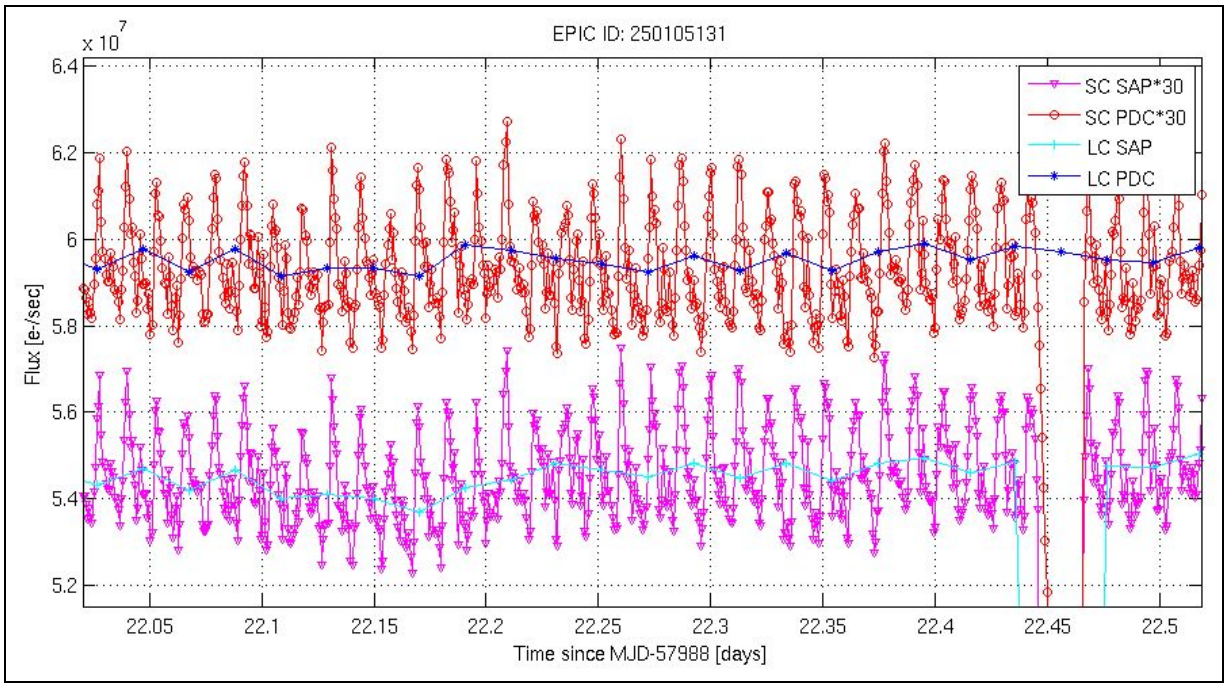

Figure 7: The C15 long- and short-cadence PA and PDC lightcurves of the AM CVn type binary HP Lip. The ~18 minute periodic photometric variation is only apparent in the short-cadence data.

2.3.2. Minor Changes

2.3.2.1. LDE Parity Error Flag

An 'LDE Parity Error' flag was set on-board the spacecraft for all targets when a bright object on that channel bled into the serial readout register area of the CCD and resulted in an out of bounds value in the analog-to-digital converter. Since this was an extremely rare event during the *Kepler* mission, the pipeline was set to discard all cadences flagged as 'LDE Parity Error' in both the target pixel and lightcurve files for all targets. With *K2*, there were many bright stars and bright, moving planets that occurred in several campaigns. This caused the 'LDE Parity Error' flag to be tripped for multiple cadences in several campaigns. Specifically, 1,237 cadences are flagged in C2 most likely due to the K_p~4 star EPIC 205283834, 128 in C6 most likely due to Spica, 148 in C11 most likely due to Saturn, and between 2–11 cadences in all other campaigns. Inspecting the cadences, the actual data was found not to be defective, and thus these cadences should ideally not be discarded.

As shown in Figure 8, the pipeline was set to discard cadences based on the 'LDE Parity Error' flag for C0, C1, C3, C4, C6, and C8. No ill effects were seen in the other campaigns when the pipeline was set to ignore the flag. Thus, for C15–C19 and all reprocessed campaigns, the pipeline was set to ignore the flag, which will result in more cadences with good data available to users.

	C0	C1	C2	C3	C4	C5	C6	C7	C8	C9	C10	C11	C12	C13	C14	C15	C16	C17	C18	C19
LDE Parity Error Flag Ignored	✓	✓	✓	✓		✓		✓		✓	✓	✓	✓	✓	✓	✓	✓	✓	✓	✓
Momentum Dump Flag Used	✓	✓	✓	✓	✓	✓						✓	✓	✓	✓	✓	✓	✓	✓	✓
Smear Corrected Properly	✓	✓	✓	✓	✓	✓	✓	✓	✓	✓	✓	✓	✓	✓	✓	✓	✓	✓	✓	✓
FFI Interpolation Bug Fixed	✓	✓	✓	✓	✓	✓	✓	✓	✓	✓	✓	✓	✓	✓	✓	✓	✓	✓	✓	✓
Scrambled Uncertainties Bug Fixed	✓	✓	✓	✓		✓						✓	✓	✓	✓	✓	✓	✓	✓	✓
All Target Files Delivered	✓	✓	✓	✓	✓	✓	✓	✓	✓	✓	✓	✓	✓	✓		✓	✓	✓	✓	✓

Figure 8: The status of minor processing features for each campaign as of June 3, 2019. Check marks indicate that the feature is present in the currently available data for that campaign. Blue check marks are features/improvements added as a result of the global uniform reprocessing effort. The *K2* mission will endeavor, on a best-effort basis, to fill in as many of the blank boxes as possible as the global uniform reprocessing effort continues.

2.3.2.2. Momentum Dump Flag

A “momentum dump” flag (QUALITY and SAP_QUALITY flag bit #6, decimal=32 : “Reaction wheel desaturation event”; see Appendix A) was set on-board the spacecraft for all targets when the spacecraft initiated a momentum dump (a.k.a. a 're-sat'). This happened about every 2 days as part of normal *K2* operations to maintain spacecraft pointing with two reaction wheels. During this time, the spacecraft would move up to half a degree within a cadence, which will significantly affect the ability to measure accurate photometry during an affected cadence.

The *Kepler* pipeline was nominally set to discard cadences flagged as 'Momentum Dump' in both the target pixel and lightcurve files. As shown in Figure 8, the pipeline utilized the 'Momentum Dump' flag for C0–C5 and C11–C14. For C6–C10, the mission experimented with setting the pipeline to ignore the flag, as there was a possibility that some of these flagged cadences did not have significant motion and might produce accurate photometry. However, upon examination based on the C6–C10 data, the mission found that indeed these flagged cadences should be discarded and accurate photometry was not able to be recovered for them. Thus, for C15–C19, as well as all reprocessed campaigns, the pipeline discarded cadences flagged as 'Momentum Dump' (QUALITY and SAP_QUALITY bit #6, decimal value = 32) in both the target pixel and lightcurve files. This will result in ~40 fewer cadences for C6–C10, but likely improved light curves as PDC will be able to better detrend the data without having to spend power on correcting flux outliers as a result of the momentum dumps.

2.3.2.3. C13 Smear Coefficient

In C13, the 1st magnitude star Aldebaran on channel 73 bled heavily into the serial register of the CCD, corrupting the first three rows of the masked smear region. While these rows were not used for the smear correction, at times during C13 the saturation spill covered more rows in the masked smear, extending up to row 15 on channel 74. Trailing black rows 7-18 were fit with a linear model to estimate the black (bias)

level for the masked smear region. At these times, the trailing black estimate for the masked smear signal was corrupted, resulting in corrupted black and smear measurements for the affected cadences. Since the black signal was subtracted from all the pixels in the channel, all targets on channel 74 were affected for these cadences, resulting in light curves that showed significant 'chatter' in baseline flux level for affected cadences. The black and smear corruption effects were most prominent in the first 80 cadences of the campaign and again in the period between cadence 1800-3200. The net effect was to render the data for targets on channel 74 in C13 nearly unusable for science study (without significant work by users to recalibrate the pixel data).

As shown in Figure 8, under "Smear Corrected Properly", this effect was unique to C13. When C13 was reprocessed, the black level model coefficients for channel 74 were manually set to reasonable values for all cadences, thus producing nominal data for all targets on channel 74.

2.3.2.4. Full-Field Image (FFI) Interpolation Bug

When a *K2* campaign had more than one Full-Field Image, the *Kepler* pipeline interpolates data between those FFIs, and extrapolates before and after each, to account for variations over time when calibrating the pixel-level data. A bug was discovered where FFIs from later campaigns were used to interpolate for calibration of the current campaign. Since there are usually two FFIs per campaign, taken ~1/3 and ~2/3 the way through, this bug affected the pixel-level data (and thus lightcurves and other products as well) for the last ~1/3 of a campaign, where the interpolation was between the last FFI of the current campaign and the first FFI of the next campaign (with a different field-of-view). The latest cadences of the campaign are affected the most. The exact impact of the effect is not known, but is thought to be small given that the FFI data are only used to supplement the undershoot correction (see KIH §6.6) in calibration and the interpolation will weight the FFI values towards the correct campaign.

As shown in Figure 8, because campaigns were predominantly processed in the order they were observed, this bug only affected C1 and C2, which were processed when FFIs for later campaigns were already ingested. The bug was fixed in the pipeline code and C1 and C2 were reprocessed.

2.3.2.5. Scrambled Uncertainties

A bug in the *Kepler* pipeline was discovered that caused the uncertainties on the smear calibration data for each column to be randomly scrambled, i.e., while each column's smear value was correct, it had a random uncertainty from another column, which can vary by ~20% column-to-column. When these uncertainties are propagated into the pixel-level flux value uncertainties, it results in incorrect flux uncertainties on the level of ~0.3%. The biggest impact this has is on the selection of the optimal photometric aperture, the algorithm for which is known to be overly sensitive to the uncertainties. Tests performed by the mission with the bug present versus the bug fixed confirm that while the bug had no significant effect on overall photometric precision, it did cause a significant change in the photometric aperture selected for a small number of targets.

As shown in Figure 8, C0–C10 were affected by this bug before it was detected and corrected in time for reprocessing.

2.3.2.6. Undelivered Targets

During the initial processing for three campaigns there were various reasons that some targets did not have target-pixel and/or lightcurve data delivered. For C2, no lightcurves were delivered as the *Kepler* pipeline had not been fully adapted to work for *K2* at the time, and until the code was finalized, it was deemed best to just produce target pixel files. For C2, C11a, C11b, and C14, there were 2–3 targets each that had an error when computing their centroids such that no World Coordinate Solution (WCS) information was available and a FITS file could not be created for those targets, and thus no target pixel files nor lightcurves were delivered. For C11b, there were 191 targets that did not have delivered target pixel files or lightcurves due to a bug in how the pipeline FITS file creator was configured to run.

As shown in Figure 8, only C2, C11, and C14 had undelivered targets. For global reprocessing, all the issues mentioned above have been fixed/addressed and thus the missing targets were delivered for C2 and C11 when they were reprocessed, and will be delivered for C14 when reprocessed.

2.4. Archive Files

The *K2* archive at MAST has the same types of files and file formats as *Kepler* (KAM §2.3), with two exceptions: there are no RC (reverse-clock) data files and there is a new type of target pixel file, "Type-1." In general, file names have changed from **`kplr*.fits`** to **`ktwo*.fits`**, and minor changes to the headers (such as removal of the SEASON keyword and changing QUARTER to CAMPAIGN and MISSION to *K2*) have occurred.

In the early days of *K2*, calibrated target pixels were released while developing in parallel the software needed to produce light curves under *K2* conditions, rather than holding data releases until the upgraded light curve software was ready to be run in its entirety. These target pixel files (TPFs) are called "Type-1 TPFs." Type-1 TPFs have WCS based on a focal plane model (see KAM §2.3.5.14-16) and commanded pointing, rather than using the science data to empirically reconstruct a pointing history. The Type-1 WCS coordinates can be off by 1–2 pixels given the unmodeled roll motion and discrete pointing offsets (§3.1). See §3.4 for an independent assessment of WCS fidelity.

For the initial C3–C8 and C10b–C19 processings, as well as all reprocessed campaigns aside from C9 and C10a, later stages of the pipeline were used to empirically reconstruct the pointing history and associated thruster firings. That information is included in the TPFs, which are called "Type-2 TPFs." The standard Type-2 TPFs are part of all data releases which produce light curves, and contain WCS coordinates based on the reconstructed pointing, aberration, and local optical distortion determined from the measured PRF centroid motion of a number of bright unsaturated stars across each channel. This "motion polynomial" model (KDPH; Van Cleve, 2010) tracks the roll drift and any impulsive pointing offsets, resulting in reconstructed position errors at or below 0.1 pixel for each cadence. Just as in *Kepler*, the FITS header reports only the WCS derived from the motion polynomials for the middle cadence of the campaign, so users of *K2* data will have to use the POS_CORR centroid offsets from the corresponding light curve file to offset the WCS for individual cadence *K2* target pixel images in the Type-2 pixel files. Background is also subtracted in Type-2 TPFs, whereas it was not in Type-1 TPFs.

Type-1 TPFs were produced for C9, since most pixels were in superapertures and few stars with individual apertures were available for calculating motion polynomials. Type-1 TPFs were also produced for C10a, since the pointing error at the start of the campaign was large enough to invalidate the assigned photometric apertures. No Type-2 TPFS will be produced for C9 and C10a when reprocessed due to these unavoidable constraints.

Since the *thruster firing* flags (see Appendix A) are not populated in FITS quality flags for the Type-1 TPFs, they are being delivered in separate long-cadence and short-cadence thruster firing tables referenced in individual DRNs. Note that the *possible thruster firing* flag in Appendix A has the correct value of 524288 (= 2^{19}); an incorrect value is given in Table 2-3 of the *Kepler* Archive Manual (KDMC-10008-006).

As previously discussed in §2.3.1.1 ('Dynablack'), TPFs now have RB_LEVEL and RBTDURi keywords to indicate the presence (or not) of rolling-band artifacts in the image data. The QUALITY keyword in the TPFs now have bit #18 and bit #19 (see Appendix A) to identify which cadences may have been affected by rolling-band artifacts.

As previously discussed in §2.3.1.3 ('Coarse Pointing Flag'), the QUALITY and SAP_QUALITY keywords in the TPFs and light curve files now have bit #3 (see Appendix A) to identify cadences with significant pointing error and thus may have significant systematic photometric errors.

3. Evaluation of Performance

3.1. Pointing

Pointing stability in the *Kepler* mission was typically measured in 10's of millipixels, while that of *K2* was measured in pixels. Pointing performance was quantified using the MAR (maximum attitude residual) metric, which is a time-series of the maximum distance between the measured and requested pointing during a campaign. MAR was calculated by the pipeline Photometer Performance Assessment (PPA) Attitude Determination (PAD) module (see the KDPH). MAR is presented visually as a time series in the DRNs, while a statistical summary of the time series is shown here in Table 2. MAR includes the initial constant pointing error (the offset of the telescope's boresight from the desired field of view center) as well as *motion throughout the campaign* (the roll angle change due to photon pressure and thruster firings); roughly speaking, the 10th percentile MAR is the constant part and the difference between the 10th and 90th percentiles quantifies the variation of MAR.

Table 2: Summary statistics of the Maximum Attitude Residual (MAR) in science pixels for each campaign. The 90th percentile MAR is noticeably worse in C7 than the other campaigns, while in C13 ~2% percent of cadences were afflicted by anomalous thruster firings, as discussed in detail in the C7 and C13 DRNs. There are no MAR statistics for C9 and C10a since light curves were not generated and the PPA-PAD module was therefore not run. Gapped data are excluded from these statistics.

C	10th p	median	90th p	99th p	max
0	0.42	0.91	1.42	1.85	4.99
1	0.25	0.61	1.13	1.55	1.92
2	0.22	0.58	1.16	1.64	4.72
3	0.28	0.58	1.10	1.68	2.06
4	0.19	0.49	0.96	1.41	1.99
5	0.38	0.77	1.28	1.61	1.86
6	0.33	0.60	1.15	1.63	2.12
7	0.25	0.92	1.84	2.65	3.37
8	0.27	0.64	1.25	1.74	2.29
10b	0.41	0.70	1.16	1.51	1.69
11a	0.49	0.95	1.48	1.95	2.19
11b	0.39	0.90	1.50	1.84	2.13
12	0.31	0.67	1.17	1.65	3.17
13	0.34	0.66	1.18	1.94	3.26
14	0.17	0.49	0.94	1.30	1.65
15	0.34	0.79	1.53	1.97	2.34
16	0.53	0.86	1.35	1.78	2.24
17	0.10	0.45	1.02	1.61	1.95
18	0.38	0.76	1.28	1.60	4.58
19	0.42	0.69	1.10	1.32	1.42

3.2. CDPP for Pipeline Light Curves

Combined Differential Photometric Precision (CDPP) is the effective noise in the transit detection process (Christiansen et al. 2012). In addition to instrumental factors, CDPP depends on the duration of the transit, the magnitude of the star, and the star's intrinsic variability. The natural benchmark CDPP for *Kepler* and *K2* is a 6-hour transit of a 12th magnitude dwarf (log g > 4.0) star, and this benchmark will be referred to throughout this document unless explicitly referencing other durations, magnitudes, or stellar types when quoting CDPP. While CDPP is in general a function of time, only the median or rms average over a time series for a given star (rms average is the default) will be referred to in this document. These per-star values can then be further summarized as percentiles over stars for a given output channel or for the FOV as a whole; for example, $CDPP_{10}$ is the 10th percentile of CDPP over all stars. Simpler noise metrics, such as a Savitsky-Golay filter (Van Cleve et al. 2016) or a running standard deviation can be used to approximate CDPP. Table 3 shows CDPP versus two important factors which can degrade light curve quality: the motion component (variable spacecraft roll angle) of MAR (90th–10th percentile), and the presence of bright ($K_p \leq 6$) planets in the FOV.

Table 3: 12th magnitude temporal rms average CDPP for dwarf stars vs. MAR variability and bright planets. C10b result is for temporal median since mod 4 failure gap in data made other metrics unavailable. The last column gives the stellar density as EPIC stars per square degree for $11.5 < K_p < 14.5$ mag.

	MAR (pix)	CDPP (ppm)	CDPP (ppm)		
Campaign	10th-90th p	10th p	median	Bright Planets	n*
0	1.00	50.1	191.7	Jupiter	1054
1	0.88	44.8	95.3		125
2	0.94	71.2	128.7	Mars	569
3	0.82	44.2	94.8		176
4	0.77	48.4	97.2		226
5	0.89	40.2	75.2		251
6	0.82	42.2	78.7		166
7	1.58	59.2	122.3		1618
8	0.98	47.0	96.2	Uranus	133
9	-	-	-		12690
10b	0.74	43.8	111.6		128
11a	0.98	50.6	131.8		7073
11b	1.11	58.5	125.6	Saturn	7073
12	0.86	55.5	127.3	Mars	144
13	0.84	54.8	128.9		338
14	0.77	45.6	116.8		131
15	1.19	47.9	99.2		368
16	0.82	45.4	104.9	Earth	211
17	0.92	42.5	113.4		148
18	0.90	41.2	83.8		255
19	1.76	35.8	64.5	Neptune	153

Van Cleve et al. (2016) examined pipeline light curves for C3–C6 and found that $CDPP_{10}$ increases linearly with distance from the FOV center, in proportion to roll motion, while the $CDPP_{10}$ at the center of the FOV — where roll motion is least — is 30 ppm, only 25% higher than that for *Kepler*. Each DRN contains scatter plots and FOV images of CDPP, and a link to a table showing 10th percentile and median CDPP over the FOV, sorted by magnitude bin.

C10b per-star CDPPs had to be calculated using medians over time, instead of an rms average, since the PDC pipeline module (see the KDPH), which was used in all other campaigns for the CDPP calculation, does not produce a meaningful number in the presence of large data gaps, such as that caused by the failure of mod 4 in C10b.

3.3. Compression

Data compression is an essential feature of both the *Kepler* and *K2* missions since data storage and downlink bandwidth are limited by the size of the on-board Solid State Recorder (SSR) and the Earth-*Kepler* distance, which was over 1 AU when end of flight was declared. There were real consequences to the limited size of the SSR, e.g., C3 ended earlier than expected (69.2 vs. ~80 days), and in some campaigns a second FFI was not taken since the SSR filled up faster than anticipated due to poorer than expected data compression. As succinctly stated in the KDCH, "The data compression scheme involves three steps: 1) requantizing the data so that the quantization noise is approximately a fixed fraction of the intrinsic measurement uncertainty (which is dominated by shot noise for bright pixels), 2) taking the difference between each re-quantized pixel value and a baseline value that was updated once per day, and 3) entropic encoding via a length-limited Huffman table (Jenkins & Dunnuck, 2011)."

As noted in Van Cleve et al. (2016), *K2* data contains more bits of information than *Kepler* data because of image motion and the high stellar density in some regions of the sky viewed by *K2.* More information increases the number of bits per pixel (denoted as *B* in subsequent discussion*)* needed to represent the data without significant compression losses, and required the collection of *K2* baselines every 12 hours instead of 24 hours. The *Kepler B* value was between 4.6 and 5.4 bits per pixel without significant dependence on position in the FOV or stellar density. In contrast, the *K2 B* value increased roughly linearly with radial distance from the FOV center (as does roll motion), and as the square root of the number of stars per square degree (n*) until n* reaches a limit, above which *B* is insensitive to n*. Barclay (2016, private communication), following Olbers (1823), conjectured that *B* stops increasing with n* since the sky as sampled by *Kepler*'s 4.0 arcsec pixels becomes more uniform, not less, as n* increases. This "Olbers-Barclay" limit is roughly 1.2×10^4 stars per square degree for EPIC stars with $11.5 < K_p < 14.5$. The maximum contribution of n* to *B* is then 5.0 bits per pixel, and the maximum *B* for *K2* data with in-family roll errors is ~15 bits per pixel. Hence, it is always beneficial to compress the 16-bit requantized data (steps 2 and 3 described above). In regions of low n*, such as the Galactic caps, the average *B* over the FOV is roughly 7.2 bits per pixel after the introduction of the new Huffman table in C5, which is a better match to the distribution of data values in *K2*.

3.4 Fidelity of World Coordinate System (WCS)

Handberg and Lund (2017) did an independent study of the fidelity of the *K2* WCS for both Type-1 and Type-2 TPFs. They found that the absolute correction in pixels to the estimated position of targets, based on the WCS provided in target pixel files, was a function of angular distance to the FOV center (see Figure 6 of Handberg and Lund, 2017). For the Type-1 data, with a model-derived WCS, corrections could be as large as 1 pixel, while for Type-2 data (C3 and C4) the maximum correction was 0.5 pixels with typical corrections ~0.2 pixels. They conclude, for Type-2 data, "…this level of off-set should in general be small enough to correctly identify targets in the frames." Lund et al. (2015) Figure 9 shows graphically the correction of the WCS pixel positions in the original (Data Release 2) C0 Type-1 data.

Custom non-point source targets also have WCS coordinates. Even though there may not be a well-defined point source in the aperture, a centroid is nonetheless calculated to set the reference location

within each aperture (keywords CRPIX1 / CRPIX2). While this position is arbitrary, the WCS transformation is derived from the motion polynomials (Van Cleve, 2010), which are calculated from good stars on that channel, not from the custom target itself. In the end, the WCS keywords correctly describe the mapping of pixels to the sky.

3.5 SSOs

Owing to the pointing of the *Kepler* spacecraft near the ecliptic during the *K2* mission, Solar System Objects (SSOs) frequently cross the field of view. When these objects cross other *K2* targets, they can cause spurious signals in the stellar photometry. However, pointing near the ecliptic also presents an opportunity for *K2* to characterize the light curves of SSOs, uniquely for long, uninterrupted durations. *K2* targeted many SSOs using tiled masks, in order to extract photometry of solar system objects.

K2 observed several kinds of SSOs, including planets (e.g., Uranus and Neptune), moons (e.g., Calisto), comets (e.g., Siding Springs) and asteroids (e.g., 2007 OR10). These different objects required different observational strategies, owing to their difference in brightness and astrometry. For example, in order to observe the bright planets Uranus and Neptune, large superstamps were tiled over hundreds of pixels. Both planets saturated the detector, and so large stamps were required to encapsulate bleed columns. The moons of each planet were also captured in these large superstamps. For smaller objects, such as comets and asteroids, single pixel wide masks were tiled across the known trajectory of the object. Together these masks create an elongated track, centered on the asteroid (see Figure 5 and §2.2.4).

K2 observed many SSOs, some which were very faint, such as comets and asteroids, including some fainter than 18th magnitude (where the *Kepler* precision is 3000 ppm over 5 hours). Asteroid rotation curves have large photometric amplitudes, owing to their small size, fast rotation, and nonspherical shapes. As a result, asteroids require less precision to accurately characterize rotation rate, requiring precision of only ~1%. As such, *K2* is able to provide photometry for these objects using simple aperture photometry down to ~22 magnitude.

SSOs move at different apparent speeds, depending on their orbital separation from the Sun and position in the solar system relative to the *Kepler* spacecraft. Their motion across the detector, particularly for asteroids, can be significant during a single, long cadence exposure — up to 16 pixels of movement for the fastest object, Apophis. Thus, the PRF needs to be co-added at many different spatial points during a single cadence, reducing and averaging the noise from motion over the sub-pixel sensitivity curve. Trans-Neptunian objects (TNOs) are characteristically slow and faint.

While *K2* targeted several moons, these were frequently close to extremely bright host planets (e.g., Uranus and Neptune) and were contaminated by broad PSF wings. This has made the photometry of moons observed by *K2* more noisy, and difficult to separate from the host planet photometry. Similarly, many comets may have flux from their extended coma outside their apertures and thus may pose a challenge in producing accurate photometry.

A 0- vs. 1-based indexing error in the SSO target definition algorithm was discovered in Sept. 2017, which affects all SSO data taken in C0–C15 (and was corrected for C16–C19). The observed pixels are one pixel to the left and one pixel below their correct positions, in an image orientation with the origin in the lower left, row number as the ordinate, and column number as the abscissa. In the correct tiled mask target sets, the object path should be centered in the union of target pixel masks. Note that the object path itself had the correct pixel coordinates, only the assignment of pixels was affected by the bug. While users may see this offset in movies of the object path (for example, the Pluto movie in the C7 DRN), they likely will not notice significant problems with photometry due to this bug, as the mask sizing already included 2–3 pixels margin for roll error. The PSF for these objects is 2–3 pixels wide, and so the PSF wings can extend outside of the downloaded apertures for these early campaigns. An example for Chiron in C12 is shown in Figure 9.

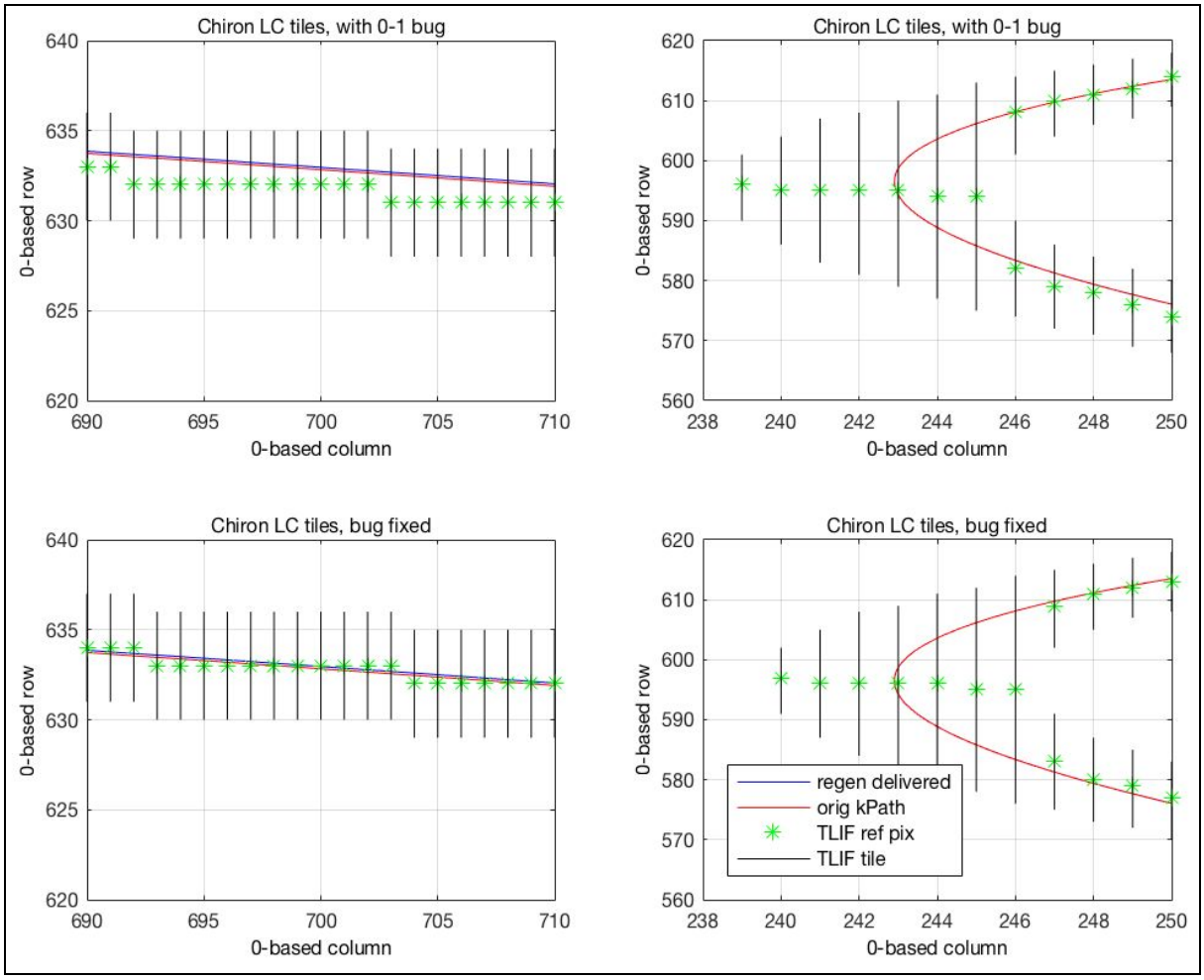

Figure 9: An example of the 0 vs. 1 based indexing error in SSO tiles using the target Chiron in C12. Upper panels: plots of the requested pixel tiles for part of Chiron's straight path (left) and at its ansa (right). Lower panels: same as the upper panels but using the corrected algorithm. The regenerated and original target paths are the blue and red lines, respectively, and show that the target path pixel coordinates were correctly calculated to better than 0.1 pixels. See the last paragraph of §3.5 (SSOs) for more details.

3.6. FGS Guide Star Variability

FGS guide star variability can potentially affect *K2* photometry by resulting in periodic pointing offsets. In C6, for example, false signals as large as 1000 ppm were impressed on light curves by the telescope motion induced by a variable guide star, as discussed in the C6 DRN and its more technical addendum[4]. Users wishing to investigate this topic further should see §4.3.

3.7. Spurious Frequencies

There are a number of sources of spurious frequencies that present themselves in long-cadence *and* short-cadence data and may significantly affect scientific analyses (e.g., asteroseismology) — short-cadence is usually affected far more significantly than long-cadence.

[4] https://keplerscience.arc.nasa.gov/images/release-notes/c6/var_fgs_kso-391_drnC6_addendum_16040722.pdf

The normalized short-cadence Simple Aperture Photometry (SAP) flux light curve of the *K2* Campaign 5 target EPIC 211414081 is shown in Figure 10. The target is a bright (K_p = 12.447 mag) star that was selected as part of an asteroseismology study. This star should be quiet and have a nice clean and (mostly) flat light curve, but the SAP flux light curve shows the effect of the star moving in and out of its pipeline-selected "optimal" aperture (OA) due to the rolling of the spacecraft caused by solar photon pressure. (Note that the size of the "optimal" aperture is calculated to strictly minimize the photometric Poisson noise on 6-hour time scales; see Smith et al. 2016). During normal *K2* operations, target starlight from the wings of the Point Spread Function (PSF) will slowly exit the OA while contaminating light from nearby stars may enter from the other side of the OA. Smaller photometric variations also result from both inter- and intra-pixel sensitivity variations as the target star moves from pixel to pixel (Vorobiev, Ninkov, Caldwell, et al. 2018; Saunders, Luger, Barnes, 2019). After a thruster firing, the star returns to the center of its OA and significantly more flux is once again recorded.

The Pre-search Data Conditioning Simple Aperture Photometry (PDCSAP) flux light curve (see Figure 11) shows thruster firing processing artifacts that were incompletely corrected by the PDC module. Other custom detrending techniques may perform better than PDC on targets, though since no detrending is ever 100% perfect, the thruster firing events will affect the photometry of every target at some level.

Much (if not most) of the power seen in a PDCSAP flux periodogram of many *K2* short-cadence targets is due to thruster firings and associated harmonics which occur at characteristic frequencies / periods. Figure 12 shows the short-cadence PDCSAP flux periodogram of the lightcurve shown in Figure 11. The biggest power peak in Figure 12 has a power value of 1.8823×10^8 ppm^2 h at a period of 5.8890 ± 0.0048 hours, which is associated with the thruster firing history of Campaign 5. While the height (power) of any given power peak may well change for individual short-cadence targets within a given *K2* observation campaign, the characteristic frequencies of the power peaks apparently do not change.

Examining the data in the frequency domain, instead of period, yields more information. Figure 13 shows the frequency domain version of the periodogram of EPIC 211414081 that was shown in Figure 12. Notice that the power peaks are now evenly spaced apart in the frequency-domain. The biggest peak in Figure 13 has a power value of 6.5613×10^5 ppm^2/μHz at a frequency of 47.169 ± 0.039 μHz; these values are comparable to the strongest peaks seen in Solar-like oscillation spectra of red giant branch stars observed during the *Kepler* mission (see Figure 4 of Chaplin and Miglio, 2013).

The *K2* long-cadence sampling rate is 566.391 μHz (Gilliland et al., 2010). As previously described, immediately after every 12th *K2* long-cadence observation the *Kepler* spacecraft may fire thrusters to restore pointing accuracy. One-twelfth of the *K2* long-cadence sampling rate is 47.1993 μHz. That frequency is within one standard deviation of the frequency bin with the peak power seen in Figure 13. The red bars at the bottom of Figure 13 show the harmonics of a base frequency of 47.1993 μHz.

Figure 14 shows an alternative form of Figure 13. The linear-scale of the abscissa (Y axis) has been replaced with a logarithmic scale in order to show more detail at the high-frequency end of the graph. Figure 14 shows that the harmonics of the base frequency of 47.1993 μHz extends to at least 2000 μHz.

Figure 15 shows the SAP flux version of Figure 14. While there is definitely more noise (power) at lower frequencies as expected, the spurious frequencies caused by the spacecraft motion to restore pointing accuracy (thruster firings every 5.88521 hours) are the same as in the PDCSAP flux version (harmonics of 47.1993 μHz). Comparing Figure 14 with Figure 15, it appears that where PDC works, it works well in reducing noise in the light curves. In the case of EPIC 211414081 here though, as is the case for many targets, PDC does not fully correct the systematics due to thruster firings.

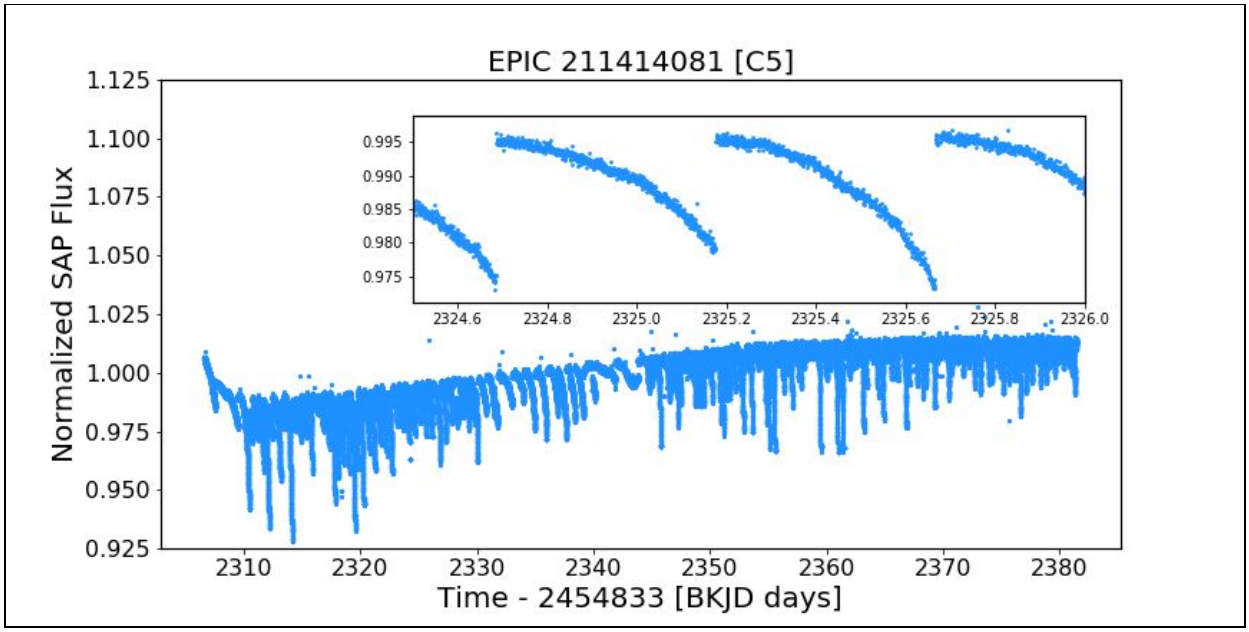

Figure 10: The normalized short-cadence SAP flux light curve of EPIC 211414081. The inset graph shows a magnified view of the effect of 3 normal thruster firings.

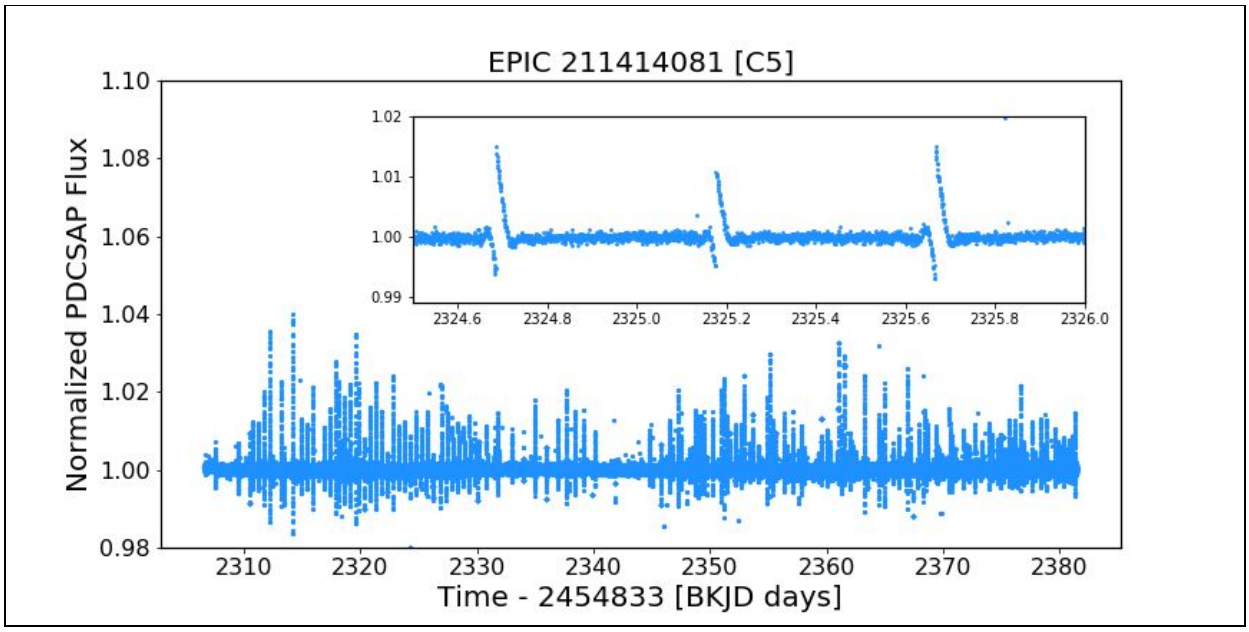

Figure 11: The normalized short-cadence PDCSAP flux detrended light curve of EPIC 211414081. The inset graph shows a magnified view of the effect of 3 normal thruster firings.

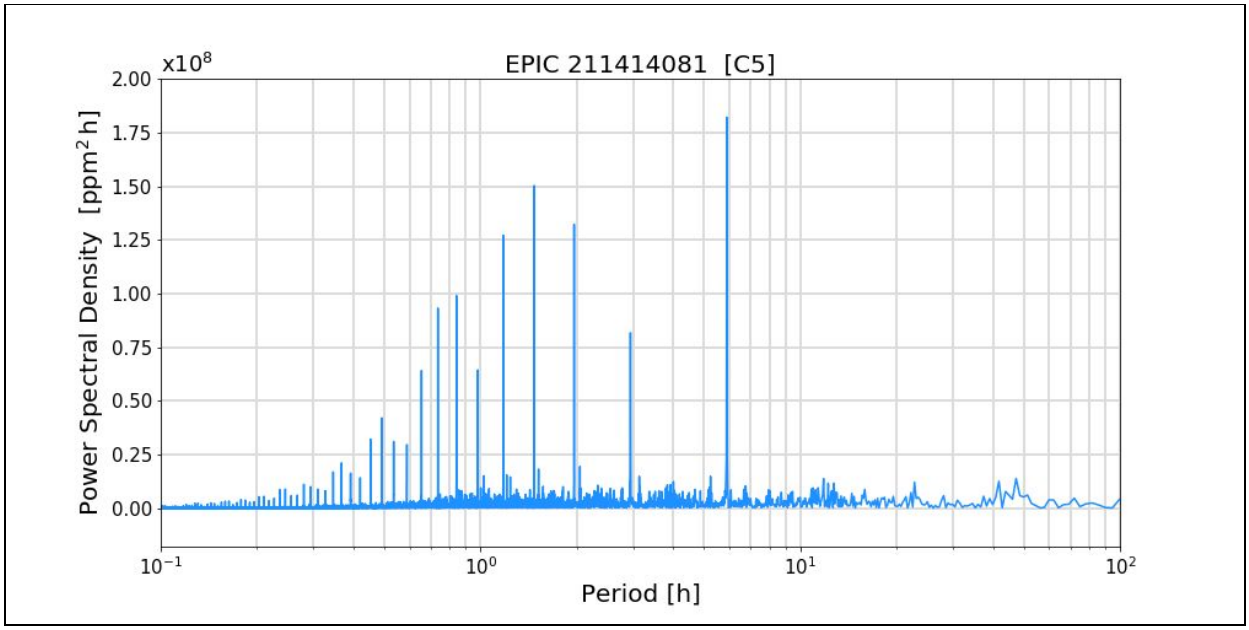

Figure 12: The short-cadence PDCSAP flux periodogram of the C5 observation of EPIC 211414081. Some of the power peaks (from right to left) occur at about 6, 3, 2, 1.5, and 1 hour.

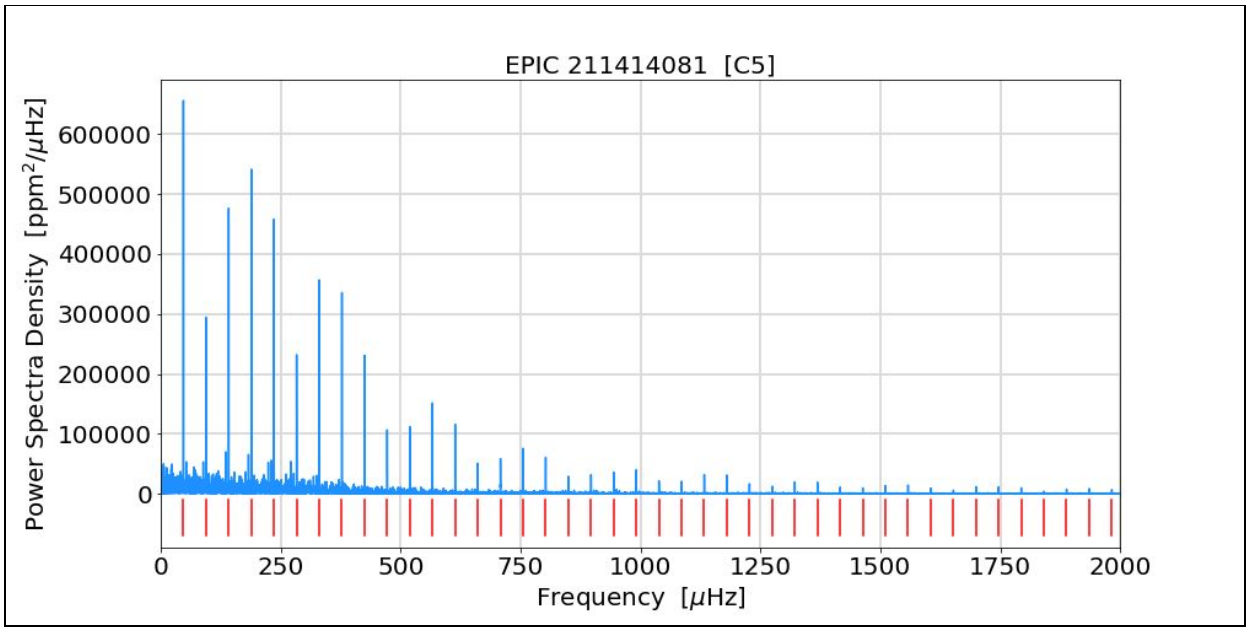

Figure 13: The short-cadence PDCSAP flux periodogram of the C5 observation of EPIC 211414081. This figure is a frequency-domain version of Figure 12. The red bars are harmonics of a base frequency of 47.1993 μHz (equivalent to a period of 5.88521 hours).

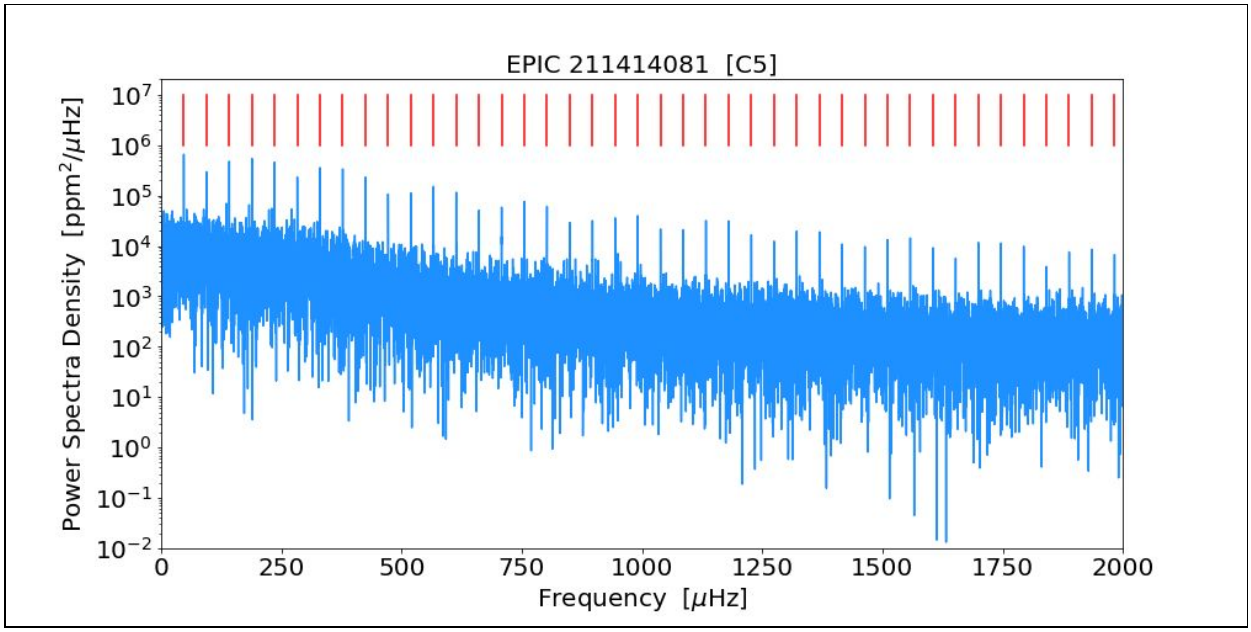

Figure 14: An alternative form (logarithmic y-axis) of the short-cadence PDCSAP flux periodogram of the C5 observation of EPIC 211414081. The red bars are harmonics of 47.1993 μHz.

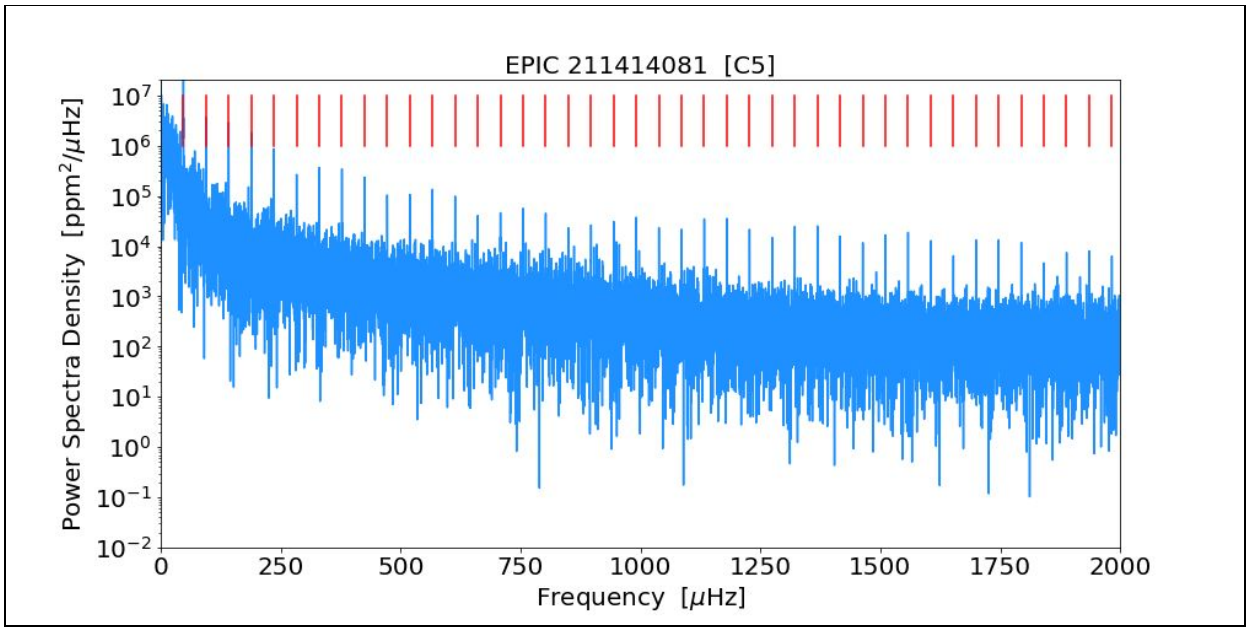

Figure 15: The SAP flux version of Figure 14. There is more noise (power) at lower frequencies, as expected with non-detrended light curves. The spurious frequencies caused by the spacecraft motion to restore pointing accuracy are, not surprisingly, the same as in the PDCSAP flux version. The red bars are harmonics of 47.1993 μHz.

While thruster firings were rare events during the *Kepler* mission, they were common during the *K2* mission in order to restore pointing accuracy of the spacecraft. *Thruster firings are by far the dominant source of spurious frequencies in K2 observations.* Even in long-cadence, PDC fluxes are affected by thruster firings; harmonics of 47.1993 μHz *below* the long-cadence Nyquist frequency of 283.2 μHz (47.1993, 94.3986, 141.5979, 188.7972, 235.9965 μHz) may well be detected.

It is worth noting that the KDCH states in §5.11.1 that for the *Kepler* mission, spurious frequencies are seen in short cadence flux times series, and pixel data of all types, including trailing black collateral pixels. The frequencies are exact multiples of the long-cadence samping rate (566.391 μHz) as seen in Figure 15 of the KDCH. Stars as bright as K_p = 9 mag may have the 8th multiple of the 1/LC artifact as the dominant spectral feature. The 1/LC artifact was first reported in *Kepler* Q1 data by Gilliland et al. (2010) and is a normal feature of the *Kepler* photometer electronics. The KDCH notes that this feature is not an artifact introduced by the pipeline, since it appears in raw trailing black collateral data. Furthermore, the feature is an additive rather than a multiplicative systematic error.

Other spurious frequencies, especially those *above* the long-cadence Nyquist frequency (283.2 μHz), were previously found in short-cadence *Kepler* observations and are summarized in KDCH §5.11.2. It is important that users be sure to check frequency detections against Table 5 of the KDCH, and do their own tests for non-astrophysical common mode signals in short-cadence data obtained with the *Kepler* photometer.

4. Engineering Data

4.1 Two-wheel Concept Engineering Test Data (E2)

The year-long transition from *Kepler* to *K2* following the reaction wheel failures is detailed in Larson et al. (2014). Part of this transition was a 9-day engineering test (E2) conducted before Campaign 0. While E2 was not intended for science, the data have been made available as uncalibrated TPFs at MAST http://archive.stsci.edu/missions/k2/eng/[5]. The E2 FOV overlaps with C12 to a large extent, so users might do their own reduction of E2 data for comparison to C12 observations to look for long-term trends in common objects. The E2 FOV was centered at (RA, DEC) = (358.5, -2.4). The filenames at MAST use non-standard Kepler IDs between 60017806 and 60044117. They are not in the EPIC, so users will have to match the RA and DECs to some other suitable catalog.

4.2 Engineering Data for Science Campaigns

The same ancillary engineering data are available at MAST for *K2* as for *Kepler* (KIH §2.5; KAM §2.3.10 and Appendix B.5). Items of particular interest are the engineering telemetry which has changed significantly between *Kepler* and *K2*, such as the roll error ADATTERRMX and the various temperatures of subsystems which experience a different thermal environment in *K2* than in the *Kepler* mission (see Appendix B.5 of the KAM for the full list). Figure 16 shows an example.

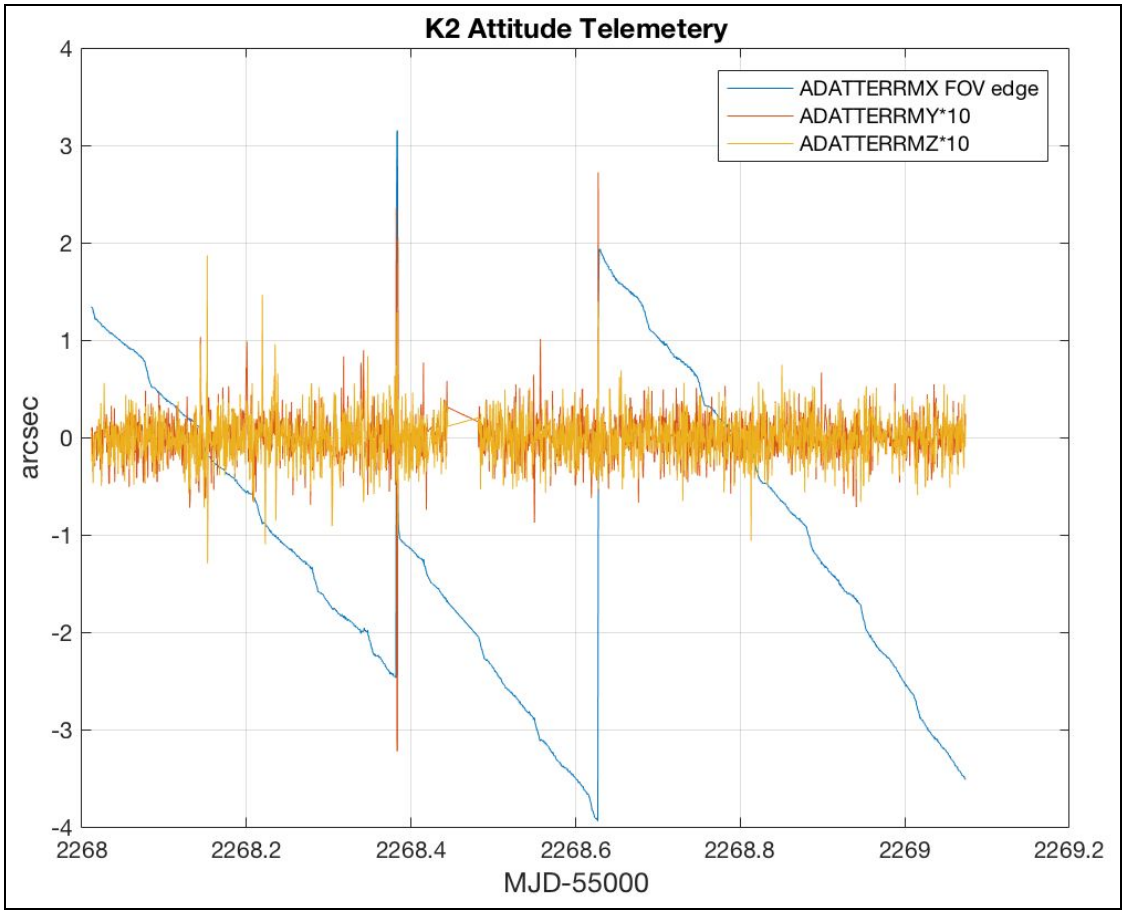

Figure 16: Example Engineering Telemetry from *K2*. ADATTERRMX is the roll about the boresight (ADATTERRMY and ADATERRMZ). It has been converted from radians to arcsec, and multiplied by the FOV radius in radians, to get the image motion in arcsec at the FOV edge.

[5] http://dx.doi.org/10.17909/t9-3gvt-3w97

4.3. FGS Data for Science Investigations

The FGS data are available at MAST for science investigations, in the form of centroid/flux time series and as (relatively infrequent) FGS FFIs. Users may find stellar variability or eclipsing binaries, or use the FGS data to more fully understand correlations and other properties of the science data. More information is available in the document KSCI-19112-002 (Mighell & Van Cleve, 2019).

4.4 Driftscan FFIs

Driftscanning was an experimental data collection mode in which the telescope collected an FFI while the telescope is drifting. A short pilot program was carried out on May 10–11, 2018 to evaluate the feasibility of this mode. Five driftscan FFIs were collected during the *K2* Campaign 17 (C17) Deep Space Network (DSN) downlink, after all C17 science data had been safely telemetered and spare DSN time remained. These five raw FFIs are available at MAST — the FFIs were never calibrated by the *Kepler*/*K2* pipeline.

Driftscanning produces long overlapping star-trails on the FFI, rather than conventional sharp point-sources. The expected length of the startrails is ~270 pixels based on an anticipated spacecraft drift motion of ~0.5 degrees per hour — the actual rate of spacecraft motion has not been measured. The direction of pointing of the telescope is not known a-priori, but can in principle be derived from the distinct constellation pattern of star trails.

The driftscan FFIs were acquired with the same combined exposure time as conventional 30-minute long cadence FFIs, i.e., 270 onboard-coadded integrations with 6.02s exposure time and 0.52s readout time per integration. The images were acquired back-to-back with gaps ranging from 30 minutes to 4 hours.

The driftscan FFIs may enhance flat-field calibration of the *Kepler* focal plane, since the relative response of adjacent pixels can be derived from the apparent variations in pixel flux as the same point spread function moved across the focal plane. Note that the detector electronics may have additional noise arising from radio frequency interference during the DSN contact.

The five driftscan FFIs are available at MAST. Their filenames are: kplr2018131024020_ffi-orig.fits, kplr2018131032646_ffi-orig.fits, kplr2018131041344_ffi-orig.fits, kplr2018131094047_ffi-orig.fits, and kplr2018131130639_ffi-orig.fits.

References

Key Websites (Links active at the time of publication)

https://archive.stsci.edu/kepler[6] (MAST-*Kepler*)
http://archive.stsci.edu/k2[7] (MAST-*K2*)
https://keplerscience.arc.nasa.gov (*K2*)

Publications

Bryson, S. T., et al. 2010a, ApJL, 713, L97
Bryson, S. T., Jenkins, J. M., Klaus, T. C. et al. 2010b, Proc. SPIE, Vol. 7740, 77401D
Christiansen, J. L., Jenkins, J. M., Caldwell, D. A., et al. 2012, PASP, 124, 1279
Chaplin, W. J., and Miglio, A. 2013, ARAA, 51, 353
Gilliland, R. L., Jenkins, J. M., Borucki, W. J., et al. 2010, ApJ, 713, L160
Handberg, R., and Lund, M. N. 2017, A&A, 597, A36
Howell, S. B., Sobeck, C., Haas, M. R., et al. 2014, PASP, 126, 398
Huber, D., Bryson, S. T., Haas, M. R., et al. 2016, ApJ Supplement, 224, 2
Jenkins, J. M., Dunnuck, J. 2011, Proc. SPIE Vol. 8146, 814602
Larson, K. A., McCalmont, K. M., Peterson, C. A., and Ross, S. E. 2014, SpaceOps 2014 Conference, SpaceOps Conferences, (AIAA 2014-1882) http://dx.doi.org/10.2514/6.2014-1882
Lund, M. N., Handberg, R., Davies, G. R., Chaplin, W. J., Jones, C. D., 2015, ApJ, 806, 30L
McCalmont, K. M., Larson, K. A., Peterson, C. A., and Ross, S. E., 2015, AIAA SPACE 2015 Conference and Exposition, doi: 10.2514/6.2015-4530
Peterson, C. A., Larson, K. A., McCalmont, K. M., and Ross, S. E., 2015, AIAA SPACE 2015 Conference and Exposition, http://arc.aiaa.org/doi/abs/10.2514/6.2015-4534
Pope, B. J. S., White, T. R., Huber, D., et al. 2016, MNRAS, 455, L36
Putnam, D., Gravseth, I., and Wiemer, D., 2106, AIAA Guidance, Navigation, and Control Conference (2016) doi: 10.2514/6.2016-0366
Rubincam, D. 2000, Icarus, 148, 2–11
Saunders, N., Luger, R., and Barnes, R., 2019, AJ, 157, 197
Smith, J. C., Morris, R. L., Jenkins, J. M., Bryson, S. T., Caldwell, D. A., Girouard, F. R. 2016, PASP, 128:124501
Szabó, Gy. M., Pál, A., Kiss, Cs., et al. 2016, A&A 599 A44
Van Cleve, J. E., Howell, S. B., Smith, J. C., et al. 2016, PASP, 128:075002
Vorobiev, D., Ninkov, Z., Caldwell, D., et al. 2018, Proc. SPIE, Vol.10698, 106985J

Kepler Mission documents available at MAST

Huber, D., and Bryson, S. T. 2019, KSCI-19082-021 "*K2*: Extending *Kepler*'s Power to the Ecliptic" (EPIC doc)
Jenkins, J. M., et al. 2017, KSCI-19081-002 "*Kepler* Data Processing Handbook" (KDPH)
Thompson, S. E., Fraquelli, D., Van Cleve, J. E., and Caldwell, D. A. 2016, KDMC-10008-006 "*Kepler* Archive Manual" (KAM)
Van Cleve, J. E., 2008, KADN-26205 "Selection of LDE Artifact Removal Pixels for Science Operations and Reverse-Clock Calibration"
Van Cleve, J. E., 2010, KADN-26285 "World Coordinate System for Target Pixel FITS Files Derived from Linearized Pipeline Motion Polynomials"
Van Cleve, J. E., and Caldwell, D. A. 2016, KSCI-19033-002, "*Kepler* Instrument Handbook" (KIH)
Van Cleve, J. E. et al. 2016, KSCI-19040-005 "Kepler Data Characteristics Handbook" (KDCH)
Mighell, K., and Van Cleve, J. E., 2017, KSCI-19112-002, "Fine Guidance Sensor Data"

[6] http://dx.doi.org/10.17909/t9-wkvz-3437

[7] http://dx.doi.org/10.17909/t9-97cz-d806

Appendix A. Revised *Kepler* Archive Manual (KAM) Table 2-3

Revised (KAM §2.3) Table 2-3 – Bits for the QUALITY and SAP_QUALITY data column.

Bit	Value	Explanation
1*	1	Attitude Tweak
2*	2	Safe Mode
3*	4	Spacecraft is in coarse point. It is set manually to pad not-in-fine point data.
4*	8	Spacecraft is in Earth point. The first real cadence after Earth point is marked.
5	16	Reaction wheel zero crossing
6*	32	Reaction wheel desaturation event
7*	64	Argabrightening detected across multiple channels on this cadence
8	128	Cosmic Ray was found and corrected in optimal aperture pixel
9*	256	Manual Exclude. The cadence was excluded because of an anomaly.
10	512	This bit is unused by *Kepler*.
11	1024	SPSD detected. This bit is flagged on the last non-gapped cadence before the maximum positive change due to the detected SPSD.
12	2048	Impulsive outlier removed before cotrending
13*	4096	Argabrightening event on specified CCD mod/out detected
14	8192	Cosmic Ray detected on collateral pixel row or column in optimal aperture.
15*	16384	Detector anomaly flag was raised.
16*	32768	Spacecraft is not in fine point.
17*	65536	No data collected.
18	131072	Rolling Band detected in optimal aperture.
19	262144	Rolling Band detected in full mask.
20	524288	Possible thruster firing. Only set in K2 data.
21	1048576	Thruster firing. Only set in K2 data.

***Indicates that these flags have been used by at least one version of the pipeline to gap data (either in CAL, PA or PDC). The original pixel level data is available in most cases.**

Appendix B. List of Acronyms

AU	Astronomical Unit
ADCS	Attitude Determination and Control Subsystem
ARP	Artifact Removal Pixel
BKJD	Barycentric *Kepler* Julian Date
CAF	Custom Aperture File
CAL	Calibration (pipeline software)
CBV	Cotrending Basis Vector
CCD	Charge Coupled Device
CDPP	Combined Differential Photometric Precision
COA	Calculate Optimal Aperture (pipeline module)
CR	Cosmic Ray
DEC	Declination
DRN	Data Release Note
EPIC	Ecliptic Plane Input Catalog
FITS	Flexible Image Transport System (digital file format)
FFI	Full Field Image
FGS	Fine Guidance Sensor
FOV	Field of View
FPA	Focal Plane Assembly
GO	Guest Observer
ID	Identifier (integer identification number)
JD	Julian Date
JPL	Jet Propulsion Laboratory
K2H	*K2* Handbook
KAM	*Kepler* Archive Manual
KIH	*Kepler* Instrument Handbook
KDCH	*Kepler* Data Characteristics Handbook
KDPH	*Kepler* Data Processing Handbook
KIC	*Kepler* Input Catalog
LC	Long Cadence
LDE	Local Detector Electronics
LGA	Low Gain Antenna
MAR	Maximum Attitude Residual
MAST	Mikulski Archive for Space Telescopes
MJD	Modified Julian Date = JD - 2400000.5
OA	Optimal Aperture
PA	Photometric Analysis (pipeline software)
PAD	Photometer Attitude Determination (pipeline software)
PDC	Pre-search Data Conditioning (pipeline software)
PDCSAP	Pre-search Data Conditioning Simple Aperture Photometry
PDF	Portable Document Format (document file format)
PPA	Photometer Performance Assessment (pipeline software)
PSF	Point Spread Function
ppm	parts per million
PRF	Pixel Response Function
RA	Right Ascension
RC	reverse-clock (pixels)
SAP	Simple Aperture Photometry
SC	Short Cadence
SCC	Short Cadence collateral
SSO	Solar System Object
SSR	Solid-State Recorder

STScI	Space Telescope Science Institute
TAD	Target and Aperture Definition
TNO	Trans-Neptunian Object
TPF	Target Pixel File
WCS	World Coordinate System
YORP	Yarkovsky-O'Keefe-Radzievskii-Paddack (effect)